

Nuclear dependence in Drell-Yan transverse momentum distribution

Xiaofeng Guo

Department of Physics, Columbia University

New York, NY 10027, USA

(November 24, 1997)

Abstract

We calculate the nuclear enhancement in Drell-Yan transverse momentum distribution in hadron-nucleus collisions. In terms of multiple scattering picture, we compute the contributions from double scattering. Applying the generalized factorization theorem, we express the nuclear enhancement in terms of twist-4 nuclear parton correlation functions. We demonstrate that these twist-4 nuclear parton correlation functions are universal, and are the same as those used to explain the nuclear dependence in di-jet momentum imbalance and in direct photon production. Using the known information on the twist-4 parton correlation functions, we estimate the nuclear enhancement for Drell-Yan pair in large q_T region. We also discuss the source of nuclear suppression in small q_T region.

11.80.La, 12.38.Bx, 13.85.Qk, 24.80.-x

Typeset using REVTeX

I. INTRODUCTION

Recently, it is found in experiment that the transverse momentum distribution of Drell-Yan pair show anomalous nuclear dependence [1]. The observed nuclear enhancement in average squared transverse momentum, $\langle q_T^2 \rangle$, grows approximately as $A^{1/3}$ with A the atomic number of the nuclear target [1,2].

Since the invariant mass of the observed Drell-Yan pairs, Q^2 , is large, it is necessary to understand the nuclear enhancement at partonic level. Any single scattering with a large Q^2 is localized in space, and hence, does not introduce the $A^{1/3}$ type nuclear dependence. The fact that the observed nuclear enhancement grows with nuclear size clearly indicate that the anomalous nuclear enhancement should be a result of multiple scattering of a parton inside the nucleus.

In terms of factorization at higher twist, Luo, Qiu and Sterman (LQS) have developed a consistent treatment of multiple scattering at partonic level [3]. LQS expressed the nuclear dependence of di-jet momentum imbalance in photo-nucleus collisions in terms of twist-4 nuclear parton distributions. Using the Fermi Lab E683 data, LQS estimated the size of the relevant twist-4 parton distributions to be of the order of $0.05 - 0.1 \text{ GeV}^2$ times typical twist-2 parton distributions [4].

The transverse momentum distribution for Drell-Yan process, $d\sigma/dQ^2 dq_T^2$, is a typical two-scale problem in perturbative QCD. When q_T^2 is the same order as Q^2 , $d\sigma/dQ^2 dq_T^2$ becomes an one scale process, and the conventional perturbative QCD calculation works well. However, when q_T^2 is much less than Q^2 , $d\sigma/dQ^2 dq_T^2$ becomes perturbatively unstable, and is proportional to $1/q_T^2$ as $q_T^2 \rightarrow 0$. In addition, the conventionally calculated partonic parts develop two powers of large logarithm, $\log^2(Q^2/q_T^2)$, for every power of α_s , due to collinear and soft gluon radiation from incoming beam partons. It is therefore necessary to perform the resummation of these large logarithms in order to get a correct Drell-Yan q_T^2 spectrum for the region when $q_T^2 \ll Q^2$ [5].

In terms of multiple scattering picture, nuclear dependence of Drell Yan q_T^2 spectrum is

a result of multiple scattering between incoming beam parton and nuclear matter before the Drell-Yan lepton pair is produced. When Q^2 and q_T^2 are both large, double scattering should be dominant. Method developed by LQS [3] can be naturally applied for calculating nuclear dependence of Drell-Yan $d\sigma/dQ^2 dq_T^2$. However, when Q^2 is large and q_T^2 is relatively small, calculating the nuclear dependence of Drell-Yan $d\sigma/dQ^2 dq_T^2$ will face the same complication as calculating $d\sigma/dQ^2 dq_T^2$ itself. As emphasized in last paragraph, when $q_T^2 \ll Q^2$, Drell-Yan $d\sigma/dQ^2 dq_T^2$ is not perturbatively stable without resummation of large logarithms. Due to possible interference of multiple scattering and collinear and soft radiation, the resummation of large logarithms may not be as straightforward [6].

Because of two physical scales, Q^2 and q_T^2 , even at lowest order, there are two types of double scattering: soft-hard double scattering and double-hard double scattering. In soft-hard process, the parton from the beam first absorbs a soft gluon at the amplitude level, and then undergoes a hard scattering with another parton from the nucleus to produce the virtual photon γ^* at Q^2 and q_T^2 . In double-hard process, the parton from the beam first undergoes a hard scattering with a parton from the nucleus to produce a quark q (or an anti-quark) at the order of q_T^2 , then the produced quark q (or anti-quark) annihilates with an anti-quark (or a quark) to produce the virtual photon at Q^2 and q_T^2 . As explained later, the double-hard process resembles the classical double scattering picture, while the soft-hard process does not. These two types of processes have opposite sign at the amplitude level. When $q_T \rightarrow 0$, the amplitude of soft-hard and double-hard scattering cancel each other. Both the soft-hard and double hard process contribute to nuclear enhancement, but their interference gives suppression effect. In large q_T region, these two processes require very different parton flux, and the interference term is less important. However, in smaller q_T region, the interference term becomes more important and can reduce the enhancement, or even give suppression effect.

In this paper, we calculate the nuclear dependence of Drell-Yan $d\sigma/dQ^2 dq_T^2$ for large q_T region, where fixed order perturbative calculation works well. Nuclear dependence in small q_T region will be addressed in Ref. [6]. This paper is organized as the following, in Sec.II, we

outline the general formalism and consideration for double scattering contribution; in Sec.III, we compute the soft-hard double scattering contributions; in Sec.IV, we derive the formula for double-hard scattering process; in Sec V, we discuss the relation between soft-hard and double-hard processes; in Sec. VI, we present the numerical result and conclusions.

II. GENERAL FORMALISM

To study the nuclear dependence of transverse momentum distribution, we consider the differential cross section for Drell-Yan process:

$$h(p') + A(p) \rightarrow \ell^+ \ell^-(q) + X , \quad (1)$$

where p' is the momentum for the incoming beam hadron, and p is the momentum per nucleon for the nuclear target. In Eq. (1), q is the four-momentum for the virtual photon, which decays into the lepton pair. In terms of contributions from multiple scattering, we expand the differential cross section as

$$\frac{d\sigma_{hA}}{dQ^2 dq_T^2 dy} = \frac{d\sigma_{hA}^S}{dQ^2 dq_T^2 dy} + \frac{d\sigma_{hA}^D}{dQ^2 dq_T^2 dy} + \dots . \quad (2)$$

The superscript ‘‘S’’ and ‘‘D’’ denote contributions from the ‘‘single scattering’’ and ‘‘double scattering’’, respectively, and ‘‘...’’ represents contributions from even higher multiple scattering. In Eq. (2), Q is the invariant mass of the lepton pair, q_T is the total transverse momentum of the lepton pair, and y is its rapidity

$$y = \frac{1}{2} \ln \frac{q_0 + q_z}{q_0 - q_z} . \quad (3)$$

As discussed above, single scattering is localized, and therefore, $d\sigma_{hA}^S/dQ^2 dq_T^2 dy$ does not contribute to anomalous nuclear dependence. It is proportional to A , modular nuclear shadowing effect. On the other hand, clear $A^{1/3}$ dependence shown in the experimental data [2] indicates that multiple scattering (higher than double scattering) is less important in proton-nucleus collisions. In this paper, we compute the double scattering contribution $d\sigma_{hA}^D/dQ^2 dq_T^2 dy$.

For fix target experiments, often the variable $x_F = 2q_z/\sqrt{s}$ is used. We can easily convert our results $d\sigma_{hA}/dQ^2 dq_T^2 dy$ to $d\sigma_{hA}/dQ^2 dq_T^2 dx_F$ by using the relation

$$dQ^2 dq_T^2 dy = \frac{1}{\sqrt{x_F^2 + 4(Q^2 + q_T^2)/s}} dQ^2 dq_T^2 dx_F . \quad (4)$$

In order to compare with experimental data, we calculate the ratio of total differential cross section and single scattering contribution,

$$R = \frac{d\sigma_{hA}}{dQ^2 dq_T^2 dy} \bigg/ \frac{d\sigma_{hA}^S}{dQ^2 dq_T^2 dy} \approx 1 + \frac{d\sigma_{hA}^D}{dQ^2 dq_T^2 dy} \bigg/ \frac{d\sigma_{hA}^S}{dQ^2 dq_T^2 dy} . \quad (5)$$

For single scattering, Fig. 1 shows the lowest order Feynman diagrams that contribute to transverse momentum distribution of Drell-Yan pair. According to factorization theorem [7], the single scattering contribution can be expressed as

$$\begin{aligned} \frac{d\sigma^S}{dQ^2 dq_T^2 dy} &= \frac{2\alpha_{em}^2 \alpha_s}{3Q^2} \sum_{a,c} \frac{1}{2s} \int \frac{dx'}{x'} \frac{dx}{x} f_{c/h}(x') f_{a/A}(x) |\overline{M}_{ca \rightarrow \gamma^*}|^2 \\ &\quad \times \frac{1}{x's + u - Q^2} \delta \left(x + \frac{x'(t - Q^2) + Q^2}{x's + u - Q^2} \right) . \end{aligned} \quad (6)$$

In Eq. (6), x' is the momentum fraction of parton ‘‘c’’ from the beam hadron h , and x is the momentum fraction of parton ‘‘a’’ from the the nuclear target. $f_{c/h}(x')$ and $f_{a/A}(x)$ are the parton distribution functions for the hadron and the nucleus respectively. s, t, u are the invariant variables defines as

$$s = (p + p')^2 = 2p \cdot p' ; \quad (7a)$$

$$t = (p' - q)^2 = -2p' \cdot q + Q^2 ; \quad (7b)$$

$$u = (p - q)^2 = -2p \cdot q + Q^2 . \quad (7c)$$

The averaged matrix element square $|\overline{M}_{ab \rightarrow \gamma^*}|^2$ can be computed from the Feynman diagrams shown in Fig. 1 [8]. For the annihilation diagram

$$|\overline{M}_{q\bar{q} \rightarrow \gamma^*}|^2 = \frac{4}{9} e_q^2 \cdot 2 \left(\frac{\hat{t}}{\hat{u}} + \frac{\hat{u}}{\hat{t}} + \frac{2Q^2 \hat{s}}{\hat{t}\hat{u}} \right) ; \quad (8a)$$

for ‘‘Compton’’ diagram with the quark from the beam and the gluon from the target

$$|\overline{M}_{gq \rightarrow \gamma^*}|^2 = \frac{1}{6} e_q^2 \cdot 2 \left(\frac{-\hat{t}}{\hat{s}} + \frac{\hat{s}}{-\hat{t}} - \frac{2Q^2 \hat{u}}{\hat{t} \hat{s}} \right) ; \quad (8b)$$

for ‘‘Compton’’ diagram with the gluon from the beam and the quark from the target

$$|\overline{M}_{gq \rightarrow \gamma^*}|^2 = \frac{1}{6} e_q^2 \cdot 2 \left(\frac{\hat{s}}{-\hat{u}} + \frac{-\hat{u}}{\hat{s}} - \frac{2Q^2 \hat{t}}{\hat{s} \hat{u}} \right) . \quad (8c)$$

In Eq. (8), the factor of coupling constants $e^4 g_s^2$ is already included in the over all factor in Eq. (6). $\hat{s}, \hat{t}, \hat{u}$ are defined as:

$$\hat{s} = (xp + x'p')^2 = xx's ; \quad (9a)$$

$$\hat{t} = (x'p' - q)^2 = x'(t - Q^2) + Q^2 ; \quad (9b)$$

$$\hat{u} = (xp - q)^2 = x(u - Q^2) + Q^2 . \quad (9c)$$

According to generalized factorization theorem [9], double scattering contribution to the cross section can be factorized into the following form:

$$\frac{d\sigma_{hA \rightarrow \bar{l}}^D}{dQ^2 dq_T^2 dy} = \sum_c \int dx' f_{c/h}(x') \frac{d\hat{\sigma}_{cA \rightarrow \bar{l}}^D}{dQ^2 dq_T^2 dy} , \quad (10)$$

where $d\hat{\sigma}_{cA}^D$ represents the double scattering contribution between a beam parton of flavor ‘‘c’’ and the nuclear target. The $f_{c/h}(x')$ is the normal twist-2 parton distribution of flavor ‘‘c’’ within a hadron ‘‘h’’. We can simplify the calculation by integrating over the leptonic part of phase space first.

$$\frac{d\hat{\sigma}_{cA \rightarrow \bar{l}}^D}{dQ^2 dq_T^2 dy} = \frac{1}{2\pi} \frac{e^2}{3Q^2} \frac{d\hat{\sigma}_{aA \rightarrow \gamma^*}}{dQ^2 dq_T^2 dy} . \quad (11)$$

According to the factorization at higher twist, $d\hat{\sigma}_{cA}^D/dQ^2 dq_T^2 dy$ can be expressed in the following factorized form:

$$\frac{d\hat{\sigma}_{cA}^D}{dQ^2 dq_T^2 dy} = \sum_i \int dx dx_1 dx_2 T_i(x, x_1, x_2, p) H_i(x, x_1, x_2, p, p', q) . \quad (12)$$

The graphical representation of Eq. (12) is shown in Fig. 2.

At lowest order, there are two types of double scattering. Fig. 3 shows sample diagrams at amplitude level for these two types of double scattering. In double scattering process,

there are two partons “a” and “b” from the nucleus participate in the scattering process. The kinematics can only fix one parton momentum. We need to integrate over the other parton’s momentum. As shown in Fig. 3, because of the extra scattering, we have two propagators, that is, two possible poles. Therefore, the leading contribution of the integration over the extra parton momentum is given by the residues at these poles. At fixed Q and q_T , we cannot have both of these two poles at the same time. The total double scattering contribution is the sum of the residue contributions from these two different poles. Correspondingly, there are two types of double scattering. Taking the residue corresponding to the pole of the first propagator, as shown in Fig. 3a, is equivalent to say that the first parton (gluon) is soft. We call it soft-hard double scattering. In this kind of processes, the parton “c” from the beam first absorbs a soft gluon at the amplitude level, and then undergoes a hard scattering with another parton from the nucleus to produce the virtual photon γ^* . The large momentum transfer occurs only in the hard scattering. Absorption of the gluon modifies the effective parton flux, so as the overall cross section. Taking the residue from the pole of the second propagator, as shown in Fig. 3b, correspond to a situation when both partons a and b have non-zero momenta. We call this kind of processes double-hard double scattering. In this type of processes, the parton “c” first have a hard scattering with a parton “b” from the nucleus to produce a quark q (or an anti-quark) at a scale of q_T^2 , then the produced quark q annihilate with an anti-quark (or a quark) “a” to produce the virtual photon at a scale of Q^2 . More discussions about the difference and the relations of soft-hard and double-hard processes is given in Sec. V. In the following two sections, we derive the contributions from soft-hard and double-hard processes respectively.

III. SOFT-HARD DOUBLE SCATTERING CONTRIBUTION

In this section, we derive the contribution from soft-hard scattering. At lowest order, the soft-hard double scattering has three types of subprocesses, as show in Fig. 4, Fig. 5 and Fig. 6. These three types of subprocesses correspond to adding two soft gluons to the

lowest order “Annihilation” and “Compton” subprocesses. In the following subsections, we present the derivations for one subprocess, and provide the results for other subprocesses.

A. Factorization and k_T expansion for soft-hard processes

Consider subprocess shown in Fig. 4. There are three independent four-momentum linking the partonic part and corresponding two-quark-two-gluon matrix element. In the center of mass frame of high energy collision, all partons inside the nucleus are moving almost parallel to each other, along the momentum of the nucleus. All three parton momenta can be approximately replaced by the components collinear to the hadron momentum. After such collinear expansion, the double scattering contribution for contribution from process shown in Fig. 4a can be written as:

$$\frac{d\hat{\sigma}_{qA\rightarrow\gamma^*}^{(SH)}}{dQ^2 dq_T^2 dy} = \frac{1}{2x's} \int dx dx_1 dx_2 \int d^2k_T \bar{T}(x, x_1, x_2, k_T, p) \bar{H}(x'p', x, x_1, x_2, k_T, p, q), \quad (13)$$

where $2x's$ is the flux factor between the incoming beam quark and the nucleus, and $x'p'$ is the momentum carried by the beam quark. We keep the k_T for the soft gluons in order to extract a double scattering contribution beyond the leading twist. The superscript “ SH ” denotes “soft-hard” double scattering. In Eq. (13), the two-quark-two-gluon matrix element, \bar{T} , is defined as

$$\begin{aligned} \bar{T}(x, x_1, x_2, k_T, p) &= \int \frac{dy^-}{2\pi} \frac{dy_1^-}{2\pi} \frac{dy_2^-}{2\pi} \frac{d^2y_T}{(2\pi)^2} \\ &\times e^{ixp^+y^-} e^{ix_1p^+y_1^-} e^{-i(x_1-x_2)p^+y_2^-} e^{-ik_T \cdot y_T} \\ &\times \frac{1}{2} \langle p_A | A^+(y_2^-, 0_T) \bar{\psi}_q(0) \gamma^+ \psi_q(y^-) A^+(y_1^-, y_{1T}) | p_A \rangle. \end{aligned} \quad (14)$$

The corresponding partonic part \bar{H} is given by the diagrams shown in Fig. 4a, with gluon lines contracted with $p^\rho p^\sigma$, quark lines from the target traced with $(\gamma \cdot p)/2$, and quark lines from the beam traced with $(\gamma \cdot (x'p'))/2$. Here, we work in Feynman gauge, in which the leading contribution from the gluon field operators is $A^\rho \approx A^+(p^\rho/p^+)$.

In order to extract the lowest order high-twist contribution, we expand the partonic part \bar{H} introduced in Eq. (13) at $k_T = 0$,

$$\begin{aligned} \overline{H}(x'p', x, x_1, x_2, k_T, p, q) &= \overline{H}(x'p', x, x_1, x_2, k_T = 0, p, q) \\ &+ \left. \frac{\partial \overline{H}}{\partial k_T^\alpha} \right|_{k_T=0} k_T^\alpha + \frac{1}{2} \left. \frac{\partial^2 \overline{H}}{\partial k_T^\alpha \partial k_T^\beta} \right|_{k_T=0} k_T^\alpha k_T^\beta + \dots \end{aligned} \quad (15)$$

In the right-hand-side of Eq. (15), the first term is the leading twist eikonal contribution, which does not correspond to physical double scattering, but simply makes the single-scattering matrix element gauge invariant. The second term vanishes after integrating over k_T . The third term will give the finite contribution to the double scattering process. Substituting Eq. (15) into Eq. (13), and integrating over d^2k_T , we obtain

$$\begin{aligned} \frac{d\hat{\sigma}_{qA \rightarrow \gamma^*}^{(SH)}}{dQ^2 dq_T^2 dy} &= \frac{1}{2x's} \int \frac{dy^-}{2\pi} \frac{dy_1^-}{2\pi} \frac{dy_2^-}{2\pi} \frac{1}{2} \langle p_A | F_\alpha^+(y_2^-) \bar{\psi}_q(0) \gamma^+ \psi_q(y^-) F^{+\alpha}(y_1^-) | p_A \rangle \\ &\times \left(-\frac{1}{2} g^{\alpha\beta} \right) \left[\frac{1}{2} \frac{\partial^2}{\partial k_T^\alpha \partial k_T^\beta} H(y^-, y_1^-, y_2^-, k_T = 0, p, q) \right]. \end{aligned} \quad (16)$$

In Eq. (16), the modified partonic part H is defined as

$$\begin{aligned} H(y^-, y_1^-, y_2^-, k_T, p, q) &= \int dx dx_1 dx_2 e^{ixp^+ y^-} e^{ix_1 p^+ y_1^-} e^{-i(x_1 - x_2) p^+ y_2^-} \\ &\times \overline{H}(x'p', x, x_1, x_2, k_T, p, q), \end{aligned} \quad (17)$$

where the partonic part \overline{H} is defined by Eq. (13), and is given by diagrams shown in Fig. 4. In Eq. (16), $F^{+\alpha} = F^{\beta\alpha} n_\beta$, and $F^{\beta\alpha}$ is the field strength, and vector $n_\beta = \delta_{\beta+}$. In obtaining Eq. (16), we use the factor $k_T^\alpha k_T^\beta$ in Eq. (15) to convert the field A^+ into field strength by partial integration.

B. Integration over the parton momentum fractions

From Eqs. (16) and (17), all integrals of x, x_1 and x_2 can now be done explicitly without knowing the details of the multi-parton matrix elements.

Consider the diagram shown in Fig. 4a. The final state photon-gluon two particle phase space can be written as

$$\Gamma^{(2)} = \frac{1}{16\pi^2} \frac{1}{x's + u - Q^2} \delta \left(x + x_1 + \frac{\hat{t} - k_T^2 - 2k_T \cdot q}{x's + u - Q^2} \right). \quad (18)$$

In deriving Eq. (18), we have omitted the factor $dQ^2 dq_T^2 dy$, due to the definition of the invariant cross section. $k_T^2 = -k_{T\alpha} k_T^\alpha$, and \hat{t} is defined in Eq. (9b).

Using Eq. (18), the contribution to \overline{H} from the diagram shown in Fig. 4a can be expressed as

$$\begin{aligned} \overline{H}_{1a} &= \frac{\alpha_s}{4\pi} C_1 \frac{1}{x's + u - Q^2} \hat{H}_{1a}(x, x_1, x_2) \\ &\times \frac{1}{x_1 - x_2 - \frac{k_T^2}{x's} - i\epsilon} \frac{1}{x_1 - \frac{k_T^2}{x's} + i\epsilon} \delta \left(x + x_1 + \frac{\hat{t} - k_T^2 - 2k_T \cdot q}{x's + u - Q^2} \right), \end{aligned} \quad (19)$$

where the subscript “1a” has following convention: “1” stands for the first type subprocess, shown in Fig. 4; “a” corresponds to diagram in Fig. 4a. In Eq. (19), the factor C_1 is an overall color factor for first type subprocess. The function \hat{H}_{1a} in Eq. (19) is given by

$$\hat{H}_{1a} = \frac{1}{4} \frac{1}{x's} \text{Tr} \left[\gamma \cdot (x'p' + k_T) \gamma \cdot p \gamma \cdot (x'p' + k_T) R_{1a}^{\beta\nu} \gamma \cdot p L_{1a}^{\alpha\mu} \right] (-g_{\alpha\beta}) (-g_{\mu\nu}), \quad (20)$$

where $R_{1a}^{\beta\nu}$ and $L_{1a}^{\alpha\mu}$ are the right and left blob, respectively, as shown in Fig. 4a. These blobs include all possible tree Feynman diagrams with the external partons shown in the figure.

Substituting Eq. (19) into Eq. (17), we obtain

$$\begin{aligned} H_{1a} &= \frac{\alpha_s}{4\pi} C_1 \frac{1}{x's + u - Q^2} \int dx_1 dx_2 dx e^{ixp^+ y^-} e^{ix_2 p^+ y_2^-} e^{ix_1 p^+ (y_1^- - y_2^-)} \\ &\times \frac{1}{x_1 - \frac{k_T^2}{x's} + i\epsilon} \frac{1}{x_1 - x_2 - \frac{k_T^2}{x's} - i\epsilon} \\ &\times \delta \left(x + x_1 + \frac{\hat{t} - k_T^2 - 2k_T \cdot q}{x's + u - Q^2} \right) \hat{H}_{1a}(x, x_1, x_2). \end{aligned} \quad (21)$$

After performing dx by the δ -function, and dx_1 and dx_2 by contour, we derive

$$\begin{aligned} H_{1a} &= (\pi\alpha_s) C_1 \frac{1}{x's + u - Q^2} e^{i\bar{x}p^+ y^-} e^{i(k_T^2/x's)p^+(y_1^- - y_2^-)} \\ &\times \theta(-y_2^-) \theta(y^- - y_1^-) \hat{H}_{1a}(\bar{x}, x_1, x_2), \end{aligned} \quad (22)$$

where the θ -functions result from the contour integrations, and the momentum fractions for the function \hat{H}_{1a} are defined as

$$\bar{x} = -\frac{\hat{t} - 2k_T \cdot q - k_T^2}{x's + u - Q^2} - \frac{k_T^2}{x's} \quad (23a)$$

$$x_1 = \frac{k_T^2}{x's}; \quad (23b)$$

$$x_2 = 0. \quad (23c)$$

Similarly, we derive contribution from the diagram shown in Fig. 4b as

$$H_{1b} = (\pi\alpha_s) C_1 \frac{1}{x's + u - Q^2} e^{ixp^+y^-} e^{i(k_T^2/x's)p^+(y_1^- - y_2^-)} \\ \times \theta(y_2^- - y_1^-) \theta(y^- - y_2^-) \hat{H}_{1b}(x, x_1, x_2) , \quad (24)$$

where x is defined as

$$x = -\frac{\hat{t}}{x's + u - Q^2} , \quad (25)$$

and x_1 and x_2 are defined in Eqs. (23b) and (23c). Similar to Eq. (20), the partonic part \hat{H}_{1b} is given by

$$\hat{H}_{1b} = \frac{1}{4} \text{Tr} \left[\gamma \cdot (x'p') R_{1b}^{\beta\nu} \gamma \cdot p L_{1b}^{\alpha\mu} \right] (-g_{\alpha\beta}) (-g_{\mu\nu}) . \quad (26)$$

The diagram shown in Fig. 4c has following contribution

$$H_{1c} = (\pi\alpha_s) C_1 \frac{1}{x's + u - Q^2} e^{ixp^+y^-} e^{i(k_T^2/x's)p^+(y_1^- - y_2^-)} \\ \times \theta(y_1^- - y_2^-) \theta(-y_1^-) \hat{H}_{1c}(x, x_1, x_2) . \quad (27)$$

In deriving Eq. (27), we used the fact that the partonic part $\hat{H}_{1c} = \hat{H}_{1b}$ when x_1 and x_2 are evaluated at the same values as listed in Eq. (23).

Combining H_{1a} , H_{1b} and H_{1c} (given in Eqs. (22), (24), and (27), respectively) together, we obtain the total contribution to H , defined in Eq. (17), from the first type diagrams shown in Fig. 4,

$$H_1 = H_{1a} + H_{1b} + H_{1c} \\ = (\pi\alpha_s) C_1 \frac{1}{x's + u - Q^2} e^{i(k_T^2/x's)p^+(y_1^- - y_2^-)} \theta(-y_2^-) \theta(y^- - y_1^-) \\ \times \left[e^{i\bar{x}p^+y^-} \hat{H}_{1a}(\bar{x}, x_1, x_2) - e^{ixp^+y^-} \hat{H}_{1a}(x, x_1, x_2) \right] . \quad (28)$$

All momentum fractions in Eqs. (28) are evaluated at the values defined in Eqs. (23) and (25). In deriving Eq. (28), we have dropped a term proportional to

$$[\theta(-y_2^-) \theta(y^- - y_1^-) - \theta(y_2^- - y_1^-) \theta(y^- - y_2^-) - \theta(y_1^- - y_2^-) \theta(-y_1^-)] \longrightarrow 0 .$$

This is because of the phase $\exp[ixp^+y^-]$ which effectively restricts $y^- \sim 1/(xp^+) \rightarrow 0$. Physically, it means that all y integrations in such term are localized, and therefore, will not give any large nuclear size enhancement.

By substituting Eq. (28) into Eq. (16), we can obtain the lowest order double scattering contribution from first type diagrams shown in Fig. 4. One important step in getting the final result is taking the derivative with respect to k_T as defined in Eq. (16). Comparing Eq. (28) with Eq. (16), and observing that

$$\left[e^{i\bar{x}p^+y^-} \hat{H}_{1a}(\bar{x}, x_1, x_2) - e^{ixp^+y^-} \hat{H}_{1a}(x, x_1, x_2) \right]_{k_T=0} = 0, \quad (29)$$

we found that the derivatives on the exponential $\exp[i(k_T^2/x's)p^+(y_1^- - y_2^-)]$ do not contribute, and that we can therefore set $\exp[i(k_T^2/x's)p^+(y_1^- - y_2^-)] = 1$ in Eq. (28). Substituting Eq. (28) into Eq. (16), we obtain

$$\begin{aligned} \frac{d\hat{\sigma}_{qA \rightarrow \gamma^*}^{(SH)}}{dQ^2 dq_T^2 dy} &= 8\pi^2 \alpha_s^2 \alpha_{em} C_1 \frac{1}{2x's} \frac{1}{x's + u - Q^2} \left(-\frac{1}{2} g^{\alpha\beta} \right) \\ &\times \frac{1}{2} \frac{\partial^2}{\partial k_T^\alpha \partial k_T^\beta} \left[T_q(\bar{x}, A) \hat{H}_{1a}(\bar{x}, x_1, x_2) - T_q(x, A) \hat{H}_{1b}(x, x_1, x_2) \right], \end{aligned} \quad (30)$$

with \bar{x} , x_1 , x_2 and x defined in Eqs. (23) and (25). In Eq. (30), $T_q(x, A)$ is the two-quark-two-gluon matrix element, and defined as [3]:

$$\begin{aligned} T_q(x, A) &= \int \frac{dy^-}{2\pi} e^{ixp^+y^-} \int \frac{dy_1^- dy_2^-}{2\pi} \theta(y^- - y_1^-) \theta(-y_2^-) \\ &\times \frac{1}{2} \langle p_A | F_\alpha^+(y_2^-) \bar{\psi}_q(0) \gamma^+ \psi_q(y^-) F^{+\alpha}(y_1^-) | p_A \rangle. \end{aligned} \quad (31)$$

C. Final results for soft-hard processes

The derivatives with respect to k_T in Eq. (30) are straightforward. It is most convenient to re-express derivatives with respect to k_T in terms of derivatives with respect to \bar{x} or x [3]. After working out the derivatives, we obtain the parton-nucleus cross section for first type soft-hard process

$$\begin{aligned}
\frac{d\hat{\sigma}_1^{(SH)}}{dQ^2 dq_T^2 dy} &= e_q^2 \sigma_0^{DY} (12\pi\alpha_s^2) \frac{1}{2x's} \frac{1}{x's + u - Q^2} \\
&\times \left\{ \left[\frac{\partial^2}{\partial x^2} \left(\frac{1}{x} T_q(x, A) H_1(x) \right) \right] \cdot \frac{2q_T^2}{(x's + u - Q^2)^2} \right. \\
&\quad \left. + \left[\frac{\partial}{\partial x} \left(\frac{1}{x} T_q(x, A) H_1(x) \right) \right] \cdot \frac{2(Q^2 - u)}{x's(x's + u - Q^2)} \right\}, \tag{32}
\end{aligned}$$

where x is given in Eq. (25), and σ_0^{DY} is the parton level Born Drell-Yan cross section

$$\sigma_0^{DY} = \frac{4\pi\alpha_{em}^2}{9Q^2}. \tag{33}$$

In Eq. (32), $H_1(x)$ is the partonic hard part

$$H_1(x) = C_1 x \hat{H}_{1a}(x, x_1 = 0, x_2 = 0), \tag{34}$$

and $\hat{H}_{1a}(x, x_1 = 0, x_2 = 0)$ is defined in Eq. (20) with $k_T = 0$. In Eq. (32), we already include the factor $(1/2\pi)(e^2/3Q^2)$ from the leptonic part of phase space (see Eq. (11)).

After convoluting Eqs. (32) with the corresponding parton distribution from the beam, we obtain double scattering contribution to $hA \rightarrow l\bar{l}$ from the first type soft-hard double scattering process

$$\frac{d\sigma_1^{(SH)}}{dQ^2 dq_T^2 dy} = \sum_q \int dx' f_{\bar{q}/h}(x') \frac{d\hat{\sigma}_1^{(SH)}}{dQ^2 dq_T^2 dy}, \tag{35}$$

where the parton level double scattering part $d\hat{\sigma}_1^{(SH)}/dQ^2 dq_T^2 dy$ is given in Eq. (32).

Following the same derivations, we obtain contributions from second type and third type processes shown in Fig. 5 and Fig. 6. For second type diagrams, the final result for second type soft-hard process contributing to $hA \rightarrow l\bar{l}$ is

$$\frac{d\sigma_2^{(SH)}}{dQ^2 dq_T^2 dy} = \sum_q \int dx' f_{q/h}(x') \frac{d\hat{\sigma}_2^{(SH)}}{dQ^2 dq_T^2 dy}, \tag{36}$$

where the parton level double scattering part $d\hat{\sigma}_2^{(SH)}/dQ^2 dq_T^2 dy$ is:

$$\begin{aligned}
\frac{d\hat{\sigma}_2^{(SH)}}{dQ^2 dq_T^2 dy} &= e_q^2 \sigma_0^{DY} (12\pi\alpha_s^2) \frac{1}{2x's} \frac{1}{x's + u - Q^2} \\
&\times \left\{ \left[\frac{\partial^2}{\partial x^2} \left(\frac{1}{x} T_g(x, A) H_2(x) \right) \right] \cdot \frac{2q_T^2}{(x's + u - Q^2)^2} \right. \\
&\quad \left. + \left[\frac{\partial}{\partial x} \left(\frac{1}{x} T_g(x, A) H_2(x) \right) \right] \cdot \frac{2(Q^2 - u)}{x's(x's + u - Q^2)} \right\}. \tag{37}
\end{aligned}$$

In Eq. (37), the four-gluon matrix element T_g is defined as [3]

$$T_g(x, A) = \int \frac{dy^-}{2\pi} e^{ixp^+y^-} \int \frac{dy_1^- dy_2^-}{2\pi} \theta(y^- - y_1^-) \theta(-y_2^-) \\ \times \frac{1}{xp^+} \langle p_A | F^{\sigma+}(y_2^-) F_{\alpha}^{+}(0) F^{+\alpha}(y^-) F_{\sigma}^+(y_1^-) | p_A \rangle . \quad (38)$$

The partonic hard part H_2 in Eq. (37) is defined as

$$H_2 = C_2 \hat{H}_{2a}(x, x_1 = 0, x_2 = 0) , \quad (39)$$

where C_2 is the overall color factor for second type diagrams. \hat{H}_{2a} is given by the diagram shown in Fig. 5, and defined as

$$\hat{H}_{2a} = \frac{1}{4} \text{Tr} \left[\gamma \cdot (x'p' + x_1p + k_T) R_{2a}^{\beta\nu} \gamma \cdot p_3 L_{2a}^{\alpha\mu} \right] (-g_{\alpha\beta}) (-g_{\mu\nu}) , \quad (40)$$

where $p_3 = x'p' + (x + x_1)p - q$ is the momentum carried by the quark going to final state.

Similarly, for the third type soft-hard process, as sketched in Fig. 6, the final result for third type soft-hard process contributing to $hA \rightarrow l\bar{l}$ is

$$\frac{d\sigma_3^{(SH)}}{dQ^2 dq_T^2 dy} = \sum_q \int dx' f_{g/h}(x') \frac{d\hat{\sigma}_3^{(SH)}}{dQ^2 dq_T^2 dy} . \quad (41)$$

where the parton level double scattering part $d\hat{\sigma}_3^{(SH)}/dQ^2 dq_T^2 dy$ is:

$$\frac{d\hat{\sigma}_3^{(SH)}}{dQ^2 dq_T^2 dy} = e_q^2 \sigma_0^{DY} (12\pi\alpha_s^2) \frac{1}{2x's} \frac{1}{x's + u - Q^2} \\ \times \left\{ \left[\frac{\partial^2}{\partial x^2} \left(\frac{1}{x} T_q(x, A) H_3(x) \right) \right] \cdot \frac{2q_T^2}{(x's + u - Q^2)^2} \right. \\ \left. + \left[\frac{\partial}{\partial x} \left(\frac{1}{x} T_q(x, A) H_3(x) \right) \right] \cdot \frac{2(Q^2 - u)}{x's(x's + u - Q^2)} \right\} . \quad (42)$$

In Eq. (42), the partonic hard part H_3 is defined as

$$H_3 = C_3 x \hat{H}_{3a}(x, x_1 = 0, x_2 = 0) , \quad (43)$$

where C_3 is the overall color factor for the third type process, and \hat{H}_{3a} is given by the diagram shown in Fig. 6, and defined as

$$\hat{H}_{3a} = \frac{1}{4} \text{Tr} \left[\gamma \cdot p R_{3a}^{\beta\nu} \gamma \cdot p_3 L_{3a}^{\alpha\mu} \right] (-g_{\alpha\beta}) (-g_{\mu\nu}) , \quad (44)$$

where p_3 is the same as that defined following Eq. (40).

The partonic short-distance hard parts, defined in Eqs. (34), (39) and (43), can be easily evaluated by calculating the corresponding Feynman diagrams. Our results are

$$H_1(x) = \frac{2}{27} \left(\frac{x - x_a}{x} \hat{\sigma}_1 + \frac{x}{x - x_a} \hat{\sigma}_2 + \frac{2x_a}{(x - x_a)} \hat{\sigma}_3 \right) \quad (45a)$$

$$H_2(x) = \frac{1}{36} \left(\hat{\sigma}_3 + \hat{\sigma}_4 - \frac{2(x - x_a)}{x^2} \frac{Q^2}{x's} \hat{\sigma}_1 \right) \quad (45b)$$

$$H_3(x) = \frac{1}{16} \left(\frac{x}{x - x_a} \hat{\sigma}_5 + \frac{x - x_a}{x} \hat{\sigma}_6 - \frac{2x_a}{(x - x_a)} \hat{\sigma}_4 \right), \quad (45c)$$

and

$$\hat{\sigma}_1 = \frac{Q^2 - u}{x's + u - Q^2} \quad (46a)$$

$$\hat{\sigma}_2 = \frac{x's + u - Q^2}{Q^2 - u} \quad (46b)$$

$$\hat{\sigma}_3 = \frac{x's}{x's + u - Q^2} \quad (46c)$$

$$\hat{\sigma}_4 = \frac{x's + u - Q^2}{x's} \quad (46d)$$

$$\hat{\sigma}_5 = \frac{x's}{Q^2 - u} \quad (46e)$$

$$\hat{\sigma}_6 = \frac{Q^2 - u}{x's} \quad (46f)$$

In Eq. (45), x_a is defined as

$$x_a = \frac{Q^2}{Q^2 - u}. \quad (47)$$

In a special case, $Q^2 = 0$, our result for soft-hard process corresponds to direct photon production [10]. In Eqs. (32), (37) and (42), the only unknown quantities are the twist-4 parton distributions defined in Eqs. (31) and (38). They were first introduced by the authors of Ref. [3]. These twist-4 parton distributions are universal functions, and as fundamental as the usual twist-2 parton distributions. They can be measured in one process and applied to another process. More discussions about these twist-4 distributions will be given in Sec. VI.

IV. DOUBLE-HARD SCATTERING CONTRIBUTION

In this section, we derive the contribution from double-hard processes. The calculations for double-hard processes are simpler than soft-hard processes. In soft-hard double scattering case, we use covariant gauge. In order to extract the contribution beyond leading-twist in the covariant gauge, we have to keep k_T for the soft gluon in collinear expansion and expand the hard-part at $k_T = 0$. For double-hard processes, since the leading behavior is twist-four contribution, we do not need to do such k_T expansion. In addition, only the symmetric diagrams contribute to double-hard scattering. At lowest order, there are three types of diagrams contributing to double-hard subprocesses, as shown in Fig. 7, Fig. 8 and Fig. 9. In the following subsections, we give the derivations for one subprocess and provide the results for other subprocesses.

A. Separation of matrix elements and partonic hard part

Consider subprocess shown in Fig. 7. Similar to soft-hard case, there are three independent four-momenta linking the partonic part and the corresponding two-quark-two-gluon matrix element. After collinear expansion, the parton-nucleus double scattering contribution for subprocess shown in Fig. 7 can be written as:

$$\frac{d\sigma_{qA \rightarrow \gamma^*}^{(DH)}}{dQ^2 dq_T^2 dy} = \frac{1}{2x's} \int dx dx_1 dx_2 \bar{T}^D(x, x_1, x_2, p) \bar{H}^{DH}(x'p', x, x_1, x_2, p, q). \quad (48)$$

The superscript “ DH ” denotes double-hard scattering. The double-hard two-quark-two-gluon matrix element, \bar{T}^D , is defined as:

$$\begin{aligned} \bar{T}^D(x, x_1, x_2, p) = & \int \frac{p^+ dy^-}{2\pi} \frac{p^+ dy_1^-}{2\pi} \frac{p^+ dy_2^-}{2\pi} e^{ixp^+ y^-} e^{ix_1 p^+ y_1^-} e^{-i(x_1 - x_2)p^+ y_2^-} \\ & \times \frac{1}{2} \frac{1}{p^+} \langle p_A | A^\sigma(y_2^-, 0_T) \bar{\psi}_q(0) \gamma^+ \psi_q(y^-) A^\rho(y_1^-) | p_A \rangle (-g_{\sigma\rho}^\perp). \end{aligned} \quad (49)$$

$(-g_{\sigma\rho}^\perp)$ represents physically polarized gluons. In Eq. (48), the partonic part \bar{H}^{DH} is given by the diagram shown in Fig. 7, with gluon lines contracted with $(-g^{\rho\sigma})/2$, quark lines from the target traced with $(\gamma \cdot p)/2$, and quark lines from the beam traced with $(\gamma \cdot (x'p'))/2$.

In order to perform the integration of momentum fractions, we rewrite the double scattering contribution defined in Eq. (49) as

$$\begin{aligned} \frac{d\hat{\sigma}_{qA\rightarrow\gamma^*}^{(DH)}}{dQdq_T^2dy} &= \frac{1}{2x's} \int \frac{dy^-}{2\pi} \frac{p^+ dy_1^-}{2\pi} \frac{p^+ dy_2^-}{2\pi} H^{DH}(y^-, y_1^-, y_2^-, p, q) \cdot \\ &\times \frac{1}{2} \langle p_A | A^\sigma(y_2^-, 0_T) \bar{\psi}_q(0) \gamma^+ \psi_q(y^-) A^\rho(y_1^-) | p_A \rangle (-g_{\sigma\rho}^\perp). \end{aligned} \quad (50)$$

In Eq. (50), the modified partonic part H^{DH} is defined as

$$\begin{aligned} H^{DH}(y^-, y_1^-, y_2^-, p, q) &= \int dx dx_1 dx_2 e^{ixp^+y^-} e^{ix_1p^+y_1^-} e^{-i(x_1-x_2)p^+y_2^-} \\ &\times \bar{H}^{DH}(x'p', x, x_1, x_2, p, q), \end{aligned} \quad (51)$$

All the integrals of the momentum fractions can now be done explicitly without knowing the details of the matrix elements.

For diagram shown in Fig. 7, the final state photon-gluon two particle phase space can be written as

$$\Gamma^{(2)} = \frac{1}{16\pi^2} \frac{1}{x's + u - Q^2} \delta\left(x + x_1 + \frac{\hat{t}}{x's + u - Q^2}\right). \quad (52)$$

Again, we neglect $dQ^2dq_T^2dy$ in the $\Gamma^{(2)}$ because of the definition of the differential cross section. Using Eq. (52), the contribution to \bar{H}^{DH} from the diagram shown in Fig. 7 can be expressed as

$$\begin{aligned} \bar{H}_1^{DH} &= \frac{1}{16\pi^2} \frac{1}{x's + u - Q^2} \delta\left(x + x_1 + \frac{\hat{t}}{x's + u - Q^2}\right) \\ &\times \left(\frac{1}{3}\right) \frac{1}{(Q^2 - u)} \frac{1}{x - x_a - i\epsilon} \frac{1}{x + x_2 - x_a + i\epsilon} \hat{H}_1^{DH}(x, x_1, x_2). \end{aligned} \quad (53)$$

where the subscript ‘‘1’’ stands for first type double hard scattering subprocess shown in Fig. 7. x_a is defined in Eq. (47). The function \hat{H}_1^{DH} in Eq. (53) can be represented by the diagram shown in Fig. 10a. It is given by

$$\hat{H}_1^{DH} = \frac{1}{4} \text{Tr} \left[\gamma \cdot x'p' R_1^{\beta\sigma} \gamma \cdot (q - x_1p) L_1^{\alpha\rho} \right] (-g_{\alpha\beta}) (-g_{\sigma\rho}), \quad (54)$$

where $R_1^{\beta\sigma}$ and $L_1^{\alpha\rho}$ are the right and left blob, respectively, as shown in Fig. 7. These blobs include all possible tree Feynman diagrams with the external partons shown in the

figure. The factor $1/3$ in Eq. (53) comes from averaging over the color of the quark which annihilates to produce γ^* . We write it out explicitly here so that the remaining color factor will be just the color factor for \hat{H}_1^{DH} , which is represented by the diagram in Fig. 10a.

Substituting Eq. (54) into Eq. (51), we perform dx_1 integration by using the δ -function, and dx, dx_2 by contour integration. We then have

$$H_1^{DH} = \frac{1}{12} \frac{1}{x's + u - Q^2} \frac{1}{(Q^2 - u)} e^{ix_a p^+ y^-} e^{ix_b p^+ (y_1^- - y_2^-)} \times \theta(-y_2^-) \theta(y^- - y_1^-) \hat{H}_1^{DH}(x, x_1, x_2), \quad (55)$$

where the θ -functions result from the contour integrations, and the momentum fractions for the function \hat{H}_1^D are

$$x = x_a = \frac{Q^2}{Q^2 - u} \quad (56a)$$

$$x_1 = x_b = -\frac{\hat{t}}{x's + u - Q^2} - x_a \quad (56b)$$

$$x_2 = 0 \quad (56c)$$

Substituting Eq. (55) into Eq. (50), we obtain

$$\begin{aligned} \frac{d\hat{\sigma}_{qA \rightarrow \gamma^*}^{(DH)}}{dQ^2 dq_T^2 dy} &= \left(\frac{8\pi^2 \alpha_s^2 \alpha_{em}}{3} \right) \frac{1}{2x's} \int \frac{dy^-}{2\pi} \frac{(p^+)^2 dy_1^- dy_2^-}{2\pi} e^{ix_a p^+ y^-} e^{ix_b p^+ (y_1^- - y_2^-)} \\ &\times \frac{1}{2} \frac{1}{(x_b p^+)^2} \langle p_A | F_{\sigma^+}(y_2^-, 0_T) \bar{\psi}_q(0) \gamma^+ \psi_q(y^-) F^{+\sigma}(y_1^-) | p_A \rangle \\ &\times \theta(-y_2^-) \theta(y^- - y_1^-) \frac{1}{x's + u - Q^2} \frac{1}{(Q^2 - u)} \hat{H}^{DH}(x, x_1, x_2). \end{aligned} \quad (57)$$

In Eq. (57), we already convert the field A^σ into field strength $F^{+\sigma}$ by partial integration.

Define the double hard matrix element [3]

$$\begin{aligned} T_{qg}^D(x_a, x_b, A) &= \frac{1}{x_b p^+} \int \frac{dy_1^-}{2\pi} \int \frac{dy^-}{4\pi} \int p^+ dy_2^- \theta(y^- - y_1^-) \theta(-y_2^-) e^{ix_a p^+ y^-} e^{ix_b p^+ (y_1^- - y_2^-)} \\ &\times \langle p_A | F_{\sigma^+}(y_2^-) \bar{\psi}_q(0) \gamma^+ \psi_q(y^-) F^{+\sigma}(y_1^-) | p_A \rangle. \end{aligned} \quad (58)$$

Substituting Eq. (58) into Eq. (57), we obtain the parton level cross section for first type double hard process

$$\begin{aligned} \frac{d\hat{\sigma}_1^{(DH)}}{dQ^2 dq_T^2 dy} &= e_q^2 \sigma_0^{DY} (4\pi\alpha_s^2) \frac{1}{x's + u - Q^2} \frac{1}{(Q^2 - u)} \\ &\times \frac{1}{2x'x_b s} T_{qg}^D(x_a, x_b, A) \hat{H}_1^{DH}, \end{aligned} \quad (59)$$

with σ_0^{DY} the parton level Drell-Yan Born cross section defined in Eq. (33), and partonic hard part \hat{H}_1^{DH} given in Eq. (54). In deriving Eq. (59), we already included the factor $(1/2\pi)(e^2/3Q^2)$ from the leptonic part of phase space.

Comparing Eq. (59) with Eq. (32), we see that the contribution from double-hard process does not have the derivative terms, while the contribution from soft-hard process depends on the derivatives of the distributions and hard part. The derivatives of x in Eq. (32) actually result from the derivatives with respect to k_T in Eq. (30). As we pointed out in Sec. III-A, for soft-hard process, the leading term when $k_T = 0$ is the leading twist eikonal contribution and does not correspond to physical double scattering. The lowest order high-twist contribution comes from the second order derivative term in k_T expansion. For double-hard process, since momentum fraction of both partons are finite, the leading contribution is already a twist-four contribution.

B. Final results for double-hard processes

Convoluting Eq. (59) with the corresponding parton distribution from the beam hadron, we obtain contribution to $hA \rightarrow l\bar{l}$ from first type double-hard process shown in Fig.7:

$$\frac{d\sigma_1^{(DH)}}{dQ^2 dq_T^2 dy} = \sum_q \int dx' f_{\bar{q}/h}(x') \frac{d\hat{\sigma}_1^{(DH)}}{dQ^2 dq_T^2 dy}, \quad (60)$$

with $d\hat{\sigma}_1^{(DH)}/dQ^2 dq_T^2 dy$ given in Eq. (59).

Following similar derivations, we obtain contributions from second and third type double-hard processes shown in Fig. 8 and Fig. 9. For contribution from second type double-hard process shown in Fig. 8, we have

$$\frac{d\sigma_2^{(DH)}}{dQ^2 dq_T^2 dy} = \sum_q \int dx' f_{g/h}(x') \frac{d\hat{\sigma}_2^{(DH)}}{dQ^2 dq_T^2 dy}. \quad (61)$$

The parton level double scattering part $d\hat{\sigma}_2^{(DH)}/dQ^2 dq_T^2 dy$ is given by

$$\begin{aligned} \frac{d\hat{\sigma}_2^{(DH)}}{dQ^2 dq_T^2 dy} &= e_q^2 \sigma_0^{DY} (4\pi\alpha_s^2) \frac{1}{x's + u - Q^2} \frac{1}{(Q^2 - u)} \\ &\times \frac{1}{2x'x_b s} T_{qg}^D(x_a, x_b, A) \hat{H}_2^{(DH)}. \end{aligned} \quad (62)$$

σ_0^{DY} is defined by Eq. (33). In Eq. (62), the partonic hard part $\hat{H}_2^{(DH)}$ is given by

$$\hat{H}_2^{(DH)} = \frac{1}{4} \text{Tr} \left[\gamma \cdot p_3 R_2^{\beta\sigma} \gamma \cdot (q - x_a p) L_2^{\alpha\rho} \right] (-g_{\alpha\beta}) (-g_{\sigma\rho}) . \quad (63)$$

The diagram representing $\hat{H}_2^{(DH)}$ is shown in Fig. 10b.

For the third type double-hard process, shown in Fig. 9, we have

$$\frac{d\sigma_3^{(DH)}}{dQ^2 dq_T^2 dy} = \sum_q \int dx' f_{g/h}(x') \frac{d\hat{\sigma}_3^{(DH)}}{dQ^2 dq_T^2 dy} . \quad (64)$$

And $d\hat{\sigma}_3^{(DH)}/dQ^2 dq_T^2 dy$ is given by

$$\begin{aligned} \frac{d\hat{\sigma}_3^{(DH)}}{dQ^2 dq_T^2 dy} &= e_q^2 \sigma_0^{DY} (4\pi\alpha_s^2) \frac{1}{x's + u - Q^2} \frac{1}{(Q^2 - u)} \\ &\times \frac{1}{2x'x_b s} T_{qq}^D(x_a, x_b, A) \hat{H}_3^{(DH)}. \end{aligned} \quad (65)$$

In Eq. (65), the partonic hard part $\hat{H}_3^{(DH)}$ is given by

$$\hat{H}_3^{(DH)} = \frac{1}{4} \text{Tr} \left[\gamma \cdot x_b p R_3^{\beta\sigma} \gamma \cdot (q - x_a p) L_3^{\alpha\rho} \right] (-g_{\alpha\beta}) (-g_{\sigma\rho}) . \quad (66)$$

The diagram representing $\hat{H}_3^{(DH)}$ is shown in Fig. 10c. In Eq. (65), the four-quark matrix element is defined as [3]

$$\begin{aligned} T_{qq}^D(x_a, x_b, A) &= \int \frac{dy^-}{4\pi} \int \frac{dy_1^-}{4\pi} \int p^+ dy_2^- \theta(y^- - y_1^-) \theta(-y_2^-) e^{ix_a p^+ y^-} e^{ix_b p^+ (y_1^- - y_2^-)} \\ &\times \langle p_A | \bar{\psi}_q(y_2^-) \gamma^+ \psi_q(y_1^-) \bar{\psi}_q(0) \gamma^+ \psi_q(y^-) | p_A \rangle . \end{aligned} \quad (67)$$

The partonic short-distance hard parts $\hat{H}_1^{(DH)}$, $\hat{H}_2^{(DH)}$ and $\hat{H}_3^{(DH)}$, defined in Eqs. (54), (63) and (66), can be evaluated by calculating corresponding Feynman diagrams in Fig. 10.

The results are:

$$\hat{H}_1^{(DH)} = \frac{4}{9} \left(\frac{x's}{Q^2 - u} + \frac{Q^2 - u}{x's} \right) + \frac{(x's)^2 + (Q^2 - u)^2}{(x's + u - Q^2)^2}; \quad (68a)$$

$$\hat{H}_2^{(DH)} = \frac{1}{6} \left(\frac{x's + u - Q^2}{Q^2 - u} + \frac{Q^2 - u}{x's + u - Q^2} \right) - \frac{3(x's + u - Q^2)^2 + (Q^2 - u)^2}{8(x's)^2}; \quad (68b)$$

$$\hat{H}_3^{(DH)} = \frac{4}{9} \left(\frac{x's}{x's + u - Q^2} + \frac{x's + u - Q^2}{x's} \right) + \frac{(x's)^2 + (x's + u - Q^2)^2}{(Q^2 - u)^2}. \quad (68c)$$

Eq. (68) already includes the color factor for each individual Feynman diagram.

In above derivations, the only unknown quantities are double-hard matrix elements T_{qg}^D and T_{qq}^D , defined in Eqs. (58) and (67). These double-hard matrix elements are universal functions. They cannot be calculated perturbatively, but can be measured in one process and tested in another process. Theoretical predictions for double scattering can also be tested once these matrix elements are measured.

V. RELATION BETWEEN SOFT-HARD AND DOUBLE HARD SCATTERING

As discussed in Sec. II, the contributions from soft-hard processes and double-hard processes correspond to the contributions from different residues when we integrate over the parton momenta using contour integration. Let us now look at the relationship between the two kinds of double scattering process. As an example, we exam the process shown in Fig. 3. The full amplitude for the double scattering has the general form:

$$M \sim \int dx_1 \frac{1}{x_1 - x_{1a} + i\epsilon} \frac{1}{x_1 - x_{1b} + i\epsilon} F(k_T^2, x_1, x), \quad (69)$$

where x_1 is the parton momentum fraction which needs to be integrated, and x is the other parton momentum fraction. The sum of these two parton momentum fractions is fixed by the kinematics, such as $x'p'$, p_3 and q . In Eq. (69), the pole $x_1 - x_{1a}$ corresponds to the first, and $x_1 - x_{1b}$ corresponds to the second propagator, as shown in the figure. The poles are given by

$$x_{1a} = \frac{k_T^2}{x's}, \quad (70a)$$

$$x_{1b} = \frac{k_T^2 + 2p_3 \cdot k_T + 2p_3 \cdot x'p'}{x's - 2p_3 \cdot p}, \quad (70b)$$

and they are both in the same half of the complex plane in the region of interests ($x's - 2p_3 \cdot p > 0$). In Eq. (69), the function $F(k_T^2, x_1, x)$ is a non-vanishing and smooth function when $x_1 = x_{1a}$ and $x_1 = x_{1b}$. It is proportional to the parton fields of momentum at $x_1 p$ and $x p$.

When $q_T \neq 0$ and $k_T \rightarrow 0$, $x_{1a} \rightarrow 0$ while x_{1b} is finite. Using contour integration to carry out dx_1 -integral in Eq. (69), we have

$$M \sim \frac{F(k_T^2, x_{1a}, x_{tot} - x_{1a})}{x_{1a} - x_{1b}} - \frac{F(k_T^2, x_{1b}, x_{tot} - x_{1b})}{x_{1a} - x_{1b}} \sim M_{soft-hard} - M_{double-hard} , \quad (71)$$

where x_{tot} is the sum of the total mometum fraction from the target, and is a function of x' , p_3 and q . Note that in Eq. (71), the amplitude of these two terms have the opposite sign. The square of these two terms gives the leading high-twist contribution of double scattering. Square of the first term corresponds to the soft-hard double scattering case, and square of the second term corresponds to the double-hard double scattering case as we derived in the last two sections. As we will discuss later, the interference term is small when q_T is large.

When $q_T = 0$, $p_{3T} = k_T$, and the two poles given in Eq. (70) become

$$x_{1a} = \frac{k_T^2}{x's} , \quad (72a)$$

$$x_{1b} = \frac{x'\sqrt{s}/(2p_{3z}) - 1}{x's - 2\sqrt{s}p_{3z} - \sqrt{s}k_T^2/(2p_{3z})} k_T^2 \approx \frac{k_T^2}{2\sqrt{s}p_{3z}} . \quad (72b)$$

As $k_T \rightarrow 0$, both x_{1a} and x_{1b} vanish. To understand the region where $q_T \sim 0$ and $k_T \sim 0$, all terms proportional to x_1 (or x_{1a} , or x_{1b}) should not be included in $F(k_T^2, x_1, x = x_{tot} - x_1)$ for the leading pole contribution. Therefore, for the leading pole contribution in the region of $q_T \sim 0$ and $k_T \sim 0$, $F \sim F(x_{tot})$ and

$$M_{soft-hard} \sim \frac{F(x_{tot})}{x_{1a} - x_{1b}} \sim M_{double-hard} . \quad (73)$$

Consequently, $M \sim M_{soft-hard} - M_{double-hard}$ gives no leading contribution to double scattering when $q_T = 0$ [11].

The double-hard process corresponds to the classical double scattering picture. The contributions of double-hard processes given in Eqs. (59), (62) and (65) have the form of

$$\sigma \sim \sigma_1 \cdot \sigma_2 \cdot \frac{1}{Q^2}, \quad (74)$$

where σ_1 and σ_2 are the partonic cross section for first and second scatterings respectively. The soft-hard process does not have the corresponding classical double scattering picture, and hence the cross section does not have the form of Eq. (74). The fact that the scattering amplitude for double-hard process and soft-hard process cancel each other when $q_T = 0$ is a pure quantum effect.

From Eq. (71), we can see that the interference term of soft-hard double scattering and the double-hard double scattering will have a negative sign. That will give “suppression” effect. The interference is proportional to $F^*(k_T^2, x_{1a}, x_{tot} - x_{1a})F(k_T^2, x_{1b}, x_{tot} - x_{1b})$ or its complex conjugate. As $k_T \rightarrow 0$, $F^*(k_T^2, x_{1a}, x_{tot} - x_{1a})F(k_T^2, x_{1b}, x_{tot} - x_{1b}) \rightarrow F^*(0, 0, x_{tot})F(0, x_{1b}, x_{tot} - x_{1b})$. If $x_{1b} \neq 0$, overlap in phase space for F^* and F is clearly small because of the difference in parton momenta, while full overlap takes place when $x_{1b} \rightarrow 0$. Therefore, in large q_T region, we only consider the contribution from soft-hard and double-hard process respectively, and neglect the interference between them. However, in smaller q_T region, one of the two hard partons in the double-hard amplitude will become softer, and may have much bigger phase space to overlap with the soft-hard amplitude. Consequently, the interference term may become important and give large suppression effect. In order to obtain correct q_T dependence for smaller q_T region, we need to consider the interference between soft-hard and double-hard scattering as well as doing resummation of powers of $\alpha_s \ln^2(Q^2/q_T^2)$ [6].

VI. NUMERICAL RESULTS AND DISCUSSIONS

In this section, we present our numerical results for the nuclear enhancement in Drell-Yan transverse momentum distribution. We numerically evaluate the ratio of differential cross section to single scattering contribution R defined in Eq. (5) by using our analytical results presented in Sec. III and Sec. IV.

The ratio R defined in Eq. (5) depends on contributions from both single scattering and double scattering. All these contributions depend on the non-perturbative parton distributions or multi-parton correlation functions. In deriving following numerical results, the Set-1 pion distributions of Ref. [12] are used for pion beams; and the CTEQ3L parton distributions of Ref. [13] are used for free nucleons. The twist-4 multi-parton correlation functions defined in Eqs. (31), (38), (58) and (67) have not been well-measured yet. By comparing the definitions of the soft-hard correlation functions T_q and T_g with the normal twist-2 parton distributions [14], authors of Ref. [3] proposed following approximate expressions for the twist-4 soft-hard correlation functions T_q and T_g :

$$T_i(x, A) = \lambda^2 A^{1/3} f_{i/A}(x, A) \quad (75)$$

where $i = q, \bar{q}$, and g . The $f_{i/A}$ are the effective twist-2 parton distributions in nuclei, and the factor $A^{1/3}$ is proportional to the size of nucleus. The constant λ^2 has dimensions of [energy]² due to the dimension difference between twist-4 and twist-2 matrix elements. The value of λ^2 should be determined by experimental measurement. It was estimated in Ref. [4] by using the measured nuclear enhancement of the momentum imbalance of two jets in photon-nucleus collisions [15,16], and was found to be order of

$$\lambda^2 \sim 0.05 - 0.1 \text{GeV}^2 . \quad (76)$$

This value is not too far away from the naive expectation from the dimensional analysis, $\lambda^2 \sim \Lambda_{\text{QCD}}^2$. The theoretical predictions for the nuclear dependence in direct photon production base on this value was consistent with the experiment [10]. In our calculation below, we use $\lambda^2 = 0.05 \text{ GeV}^2$.

From the definition of the correlation functions in Eqs. (31) and (38), the lack of oscillation factors for both y_1^- and y_2^- integrals can in principle give nuclear enhancement proportional to $A^{2/3}$. The $A^{1/3}$ dependence is a result of the assumption that the positions of two field strengths (at y_1^- and y_2^- , respectively) are confined within one nucleon.

For double-hard matrix elements T_{qg} and T_{qq} defined in Eqs. (58) and (67), we adopt the model of Ref. [17] and take

$$T_{qg}(x_a, x_b, A) = \frac{C}{2\pi} A^{4/3} f_q(x_a) f_g(x_b) ; \quad (77a)$$

$$T_{q\bar{q}}(x_a, x_b, A) = \frac{C}{2\pi} A^{4/3} f_q(x_a) f_{\bar{q}}(x_b) , \quad (77b)$$

where $f_q, f_{\bar{q}}$ are normal twist-2 quark and anti-quark distribution, and f_g is a corresponding gluon distribution. $C = (0.35/8\pi r_0^2)$ GeV². r_0 is the value of nucleon radius, and $r_0 \approx 1.1 - 1.25$. Here we already convert the unit for C to GeV². The factor $(1/2\pi)$ comes from the difference in the overall factor of the definition for matrix elements in this paper and in Ref. [17].

In Eq. (75), the effective nuclear parton distributions $f_{i/A}$ should have the same operator definitions of the normal parton distributions with free nucleon states replaced by the nuclear states. For a nucleus with Z protons and atomic number A , we define

$$f_{i/A}(x, A) = A \left(\frac{N}{A} f_{i/N}(x) + \frac{Z}{A} f_{i/P}(x) \right) R_i^{\text{EMC}}(x, A) , \quad (78)$$

where $f_{i/N}(x)$ and $f_{i/P}(x)$ with $i = q, \bar{q}, g$ are normal parton distributions in a free neutron and proton, respectively; and $N = A - Z$. The factor R_i^{EMC} takes care of the EMC effect in these effective nuclear parton distributions. We adopted the R^{EMC} from Ref. [18], which fits the data well.

In Fig. 11, we show the ratio of double scattering and single scattering versus q_T . The ratio is normalized by $A^{1/3}$. The overall feature is that the ratio becomes smaller for larger Q and q_T . This is the typical behavior for high twist contribution. It is suppressed by the factor of $1/Q^2$ or $1/q_T^2$. Q and q_T are both large scales in the processes. On the other hand, we see that when q_T becomes very large, the ratio starts to rise again. This is the effect from the edge of phase space. The soft-hard double scattering contribution depends on the derivatives of the matrix elements. At edge of the phase space, the derivative term become more important. When $x \rightarrow 1$, the parton distribution $f(x)$ has $(1-x)^\alpha$ behavior, with $\alpha > 1$. As $x \rightarrow 1$, $df(x)/dx \gg f(x)$. Therefore, the double scattering contribution becomes more important at the edge of the phase space. The curve for $Q = 11$ GeV rise more steeply than the curve for $Q = 5$ GeV, because at high Q , we approaches edge of phase

space faster as we increase q_T .

Fig. 12 shows the ratios of the soft-hard and the double-hard contributions to single scattering contribution. The ratio is normalized by $A^{1/3}$. We see that the size of soft-hard and double-hard processes are comparable. At higher q_T , the ratio for soft-hard process increase, as explained above. The contribution from double-hard processes increase faster when q_T decreases. The contribution from double-hard processes depends on the product of two parton distributions as given in Eq. (77b). The momentum fractions x_a and x_b are smaller than the momentum fraction for soft-hard processes. Because of the steep increase in parton distribution for smaller momentum fraction, the contribution from double-hard processes increase faster as q_T becomes smaller.

Fig. 13 shows the comparison of double scattering contribution and single scattering contributions. The single scattering contribution is normalized by A and the double scattering contribution is normalized by $A^{4/3}$. Without extra $A^{1/3}$ factor, the double scattering contribution are small compare to the single scattering contribution. Perturbative calculation for double scattering should be reliable. Because of $A^{1/3}$ enhancement, the double scattering becomes important. As x_F increases, both double scattering contribution and single scattering contribution decreases, but double scattering contribution decreases slower than single scattering. We expect larger enhancement in larger x_F region.

In Fig. 14, we show the nuclear dependence of the q_T spectrum in large q_T region for different nuclear target: C, Ca, Fe, and W, when 800 GeV proton beam is used. The figure is plotted for R versus q_T . The quantity R is defined in Eq. (5). It is the ratio of total differential cross section and the single scattering cross section. Because of the $A^{1/3}$ enhancement for double scattering contribution, the ratio is larger for larger A .

As we discussed in the last section, when q_T is smaller, the interference between the double hard scattering and the soft-hard scattering becomes important. The interference will give suppression. We expect that the double scattering contribution will decrease as q_T decreases in smaller q_T region. Fig. 15 shows our expected ratio of double scattering contribution to single scattering contribution. The dotted curve and the curve on the right

side of the dash line is obtained by using our results presented in this paper. The curve on the left side of the dash line is our expected ratio when q_T becomes smaller. Since the integrated cross section $d\sigma/dQ^2$ has little A-dependence, and we have shown nuclear enhancement in large q_T region in this paper, we expect that there will be suppression in small q_T . In small q_T region that the interference between the soft-hard and double-hard processes becomes dominant contribution. From the figure, we see that the calculated ratio starts to rise steeply when q_T approaches 3 GeV and below. This is the sign where the large logarithms of $\alpha_s \ln^2(Q^2/q_T^2)$ and the interference become important.

In summary, both soft-hard and double-hard double scattering processes contribute to the nuclear dependence in Drell-Yan pair production. The double-hard subprocess resembles the classical double scattering picture, while the soft-hard subprocess and the cancellation of the leading double-hard and soft-hard contribution are pure quantum effect. Both types of double scattering processes give $A^{1/3}$ nuclear enhancement. However, the interference between these two types of process have the suppression effect. In large q_T region, the interference can be neglected and we have $A^{1/3}$ nuclear enhancement for Drell-Yan q_T spectrum. In smaller q_T region, the interference term becomes more important and may give nuclear suppression. Calculation of nuclear dependence of Drell-Yan process in small q_T region will be addressed in a future publication [6].

ACKNOWLEDGMENTS

I thank Jianwei Qiu and George Sterman for very helpful discussions. I also thank Xinian Wang for helpful communications about the reference on the experimental data. This work was supported by the Director, Office of Energy Research, Division of Nuclear Physics of the Office of High Energy and Nuclear Physics of the U.S. Department of Energy under contract No. DE-FG02-93ER40764.

REFERENCES

- [1] P. Bordalo, et al, NA10 Collaboration, Phys. Lett. **B193**, 373(1987)
- [2] D. M. Alde, et al, E772 Collaboration, Phys. Rev. Lett. **66**, 2285(1991)
- [3] M. Luo, J.-W. Qiu and G. Sterman, Phys. Lett. **B279**, 377 (1992); M. Luo, J.-W. Qiu and G. Sterman, Phys. Rev. **D50**, 1951 (1994).
- [4] M. Luo, J.-W. Qiu and G. Sterman, Phys. Rev. **D49**, 4493 (1994).
- [5] J. C. Collins, D. E. Soper and G. Sterman, Nucl. Phys. **B250**, 199(1985).
- [6] X. Guo, J.-W. Qiu, and G. Sterman, in preparation.
- [7] J. C. Collins, D. E. Soper and G. Sterman, in *Perturbative Quantum Chromodynamics*, ed. A. H. Mueller (World Scientific, Singapore, 1989).
- [8] For example, see R. field, *Application of Perturbative QCD* (Addison-Wesley, USA, 1989).
- [9] J.-W. Qiu and G. Sterman, Nucl. Phys. **B353** 137(1991); **B353** 105(1991).
- [10] X.-F. Guo and J.-W. Qiu, Phys. Rev. **D53**, 1164(1996).
- [11] J.-W. Qiu and G. Sterman, in *the Proceedings of First Summer Study on the Physics of Ultrarelativistic Nucleus-Nucleus Collisions at RHIC* (RHIC Summer Study '96), edited by D. E. Kahana and Y. Pang (BrookHaven National Laboratory, USA, 1996).
- [12] J. F. Owens, Phys. Rev. **D30**, 943 (1984).
- [13] H. L. Lai, *et al.*, Phys. Rev. **D51**, 4763 (1995); and references therein.
- [14] J. C. Collins and D. E. Soper, Nucl. Phys. **B194**, 445 (1982).
- [15] D. Naples, *et al.*, Phys. Rev. Lett. **72**, 2341 (1994).
- [16] M. D. Corcoran *et al.*, Phys. Lett. **B259** (1991), 209; T. Fields, Nucl. Phys. **A544**, 565

(1992).

[17] A. H. Mueller and J.-W. Qiu, Nucl. Phys. **B268**, 427(1986).

[18] C. J. Benesh, J.-W. Qiu and J. P. Vary, Phys. Rev. **C50**, 1015 (1994).

FIGURES

FIG. 1. Diagram for single scattering: a) Annihilation diagram; b) “Compton” diagram.

FIG. 2. A Graphical representation of double scattering contributions in proton-nucleus collisions.

FIG. 3. Sample Feynman diagrams contributing to next-to-leading order double scattering: (a) soft-hard process; (b) double-hard process. The circles represent the poles when we integrate over the parton momentum.

FIG. 4. First type soft-hard double scattering subprocesses: “Annihilation” diagrams corresponding to the two-quark-two-gluon matrix element; a) real diagram, b) and c) interference diagram.

FIG. 5. Second type soft-hard double scattering subprocesses: the real “Compton” diagrams corresponding to the four-gluon matrix element.

FIG. 6. Third type soft-hard double scattering subprocesses: the real “Compton” diagrams corresponding to the two-quark-two-gluon matrix element.

FIG. 7. Diagram corresponding to first type double-hard subprocess.

FIG. 8. Diagram corresponding to second type double-hard subprocess

FIG. 9. Diagram corresponding to third type double-hard subprocess

FIG. 10. Diagrams representing the partonic hard parts for double-hard processes: a) \hat{H}_1^{DH} for double-hard process shown in Fig. 7; b) \hat{H}_2^{DH} for double-hard process shown in Fig. 8; c) \hat{H}_3^{DH} for double-hard process shown in Fig. 9.

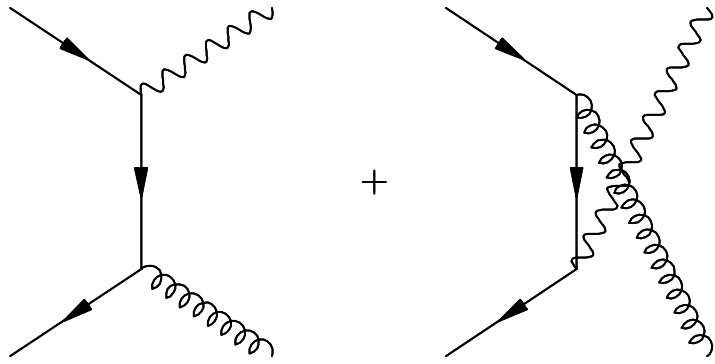
FIG. 11. The ratio of double scattering contribution and single scattering contribution normalized by $A^{1/3}$ for a 800GeV proton beam when $Q = 5\text{GeV}$ and 11GeV .

FIG. 12. The ratio of soft-hard and double-hard contributions to single scattering contribution. The ratio is normalized by $A^{1/3}$.

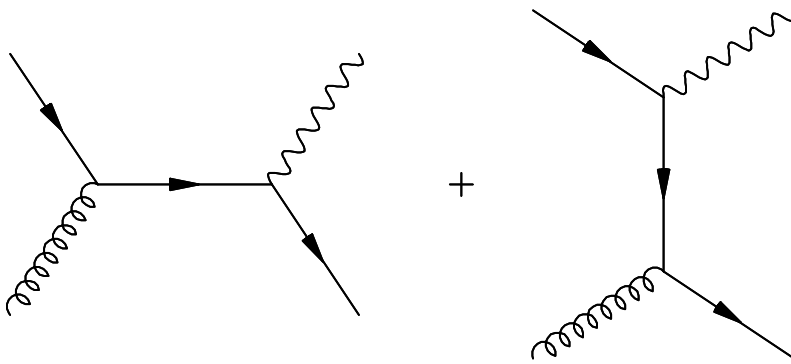
FIG. 13. Comparison of double scattering and single scattering contributions.

FIG. 14. A -dependence of q_T distribution at large q_T region for nuclear targets C, Ca, Fe and W. The quantity R is the ratio of total differential cross section and the single scattering contribution, as defined in Eq. (5).

FIG. 15. Expected ratio of double scattering to single scattering when q_T is small.



(a)



(b)

Fig.1

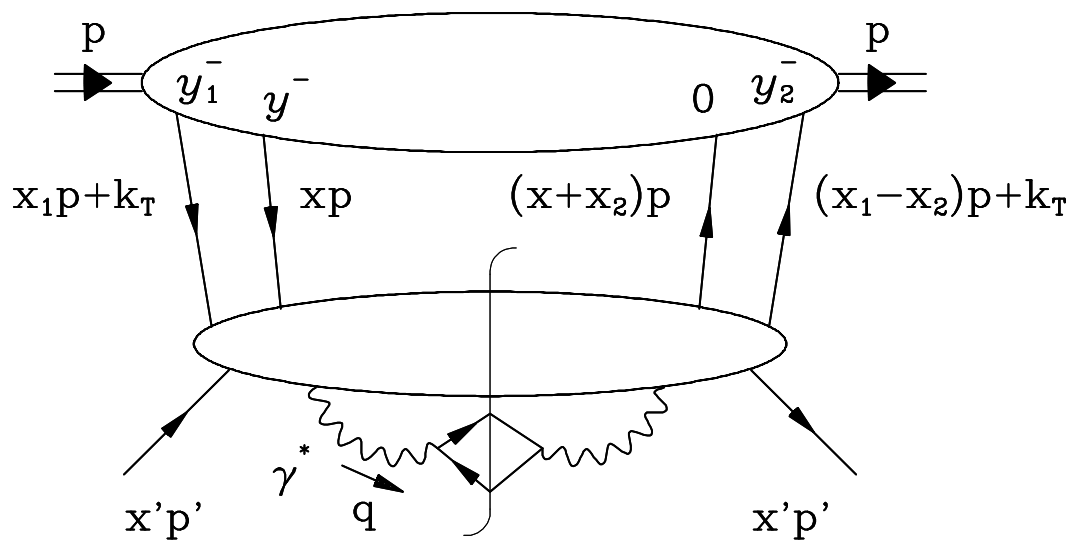
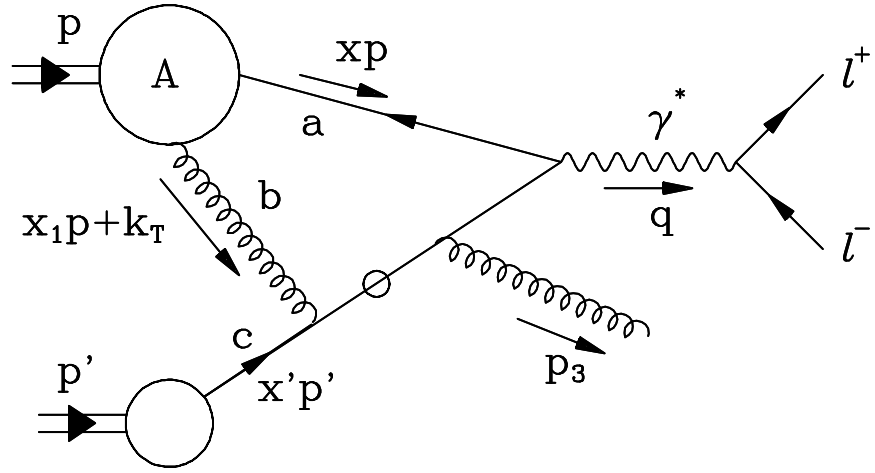
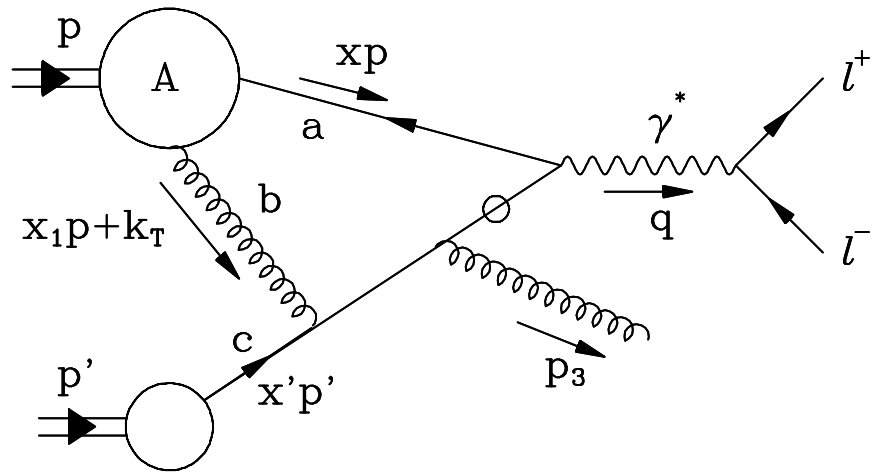


Fig.2

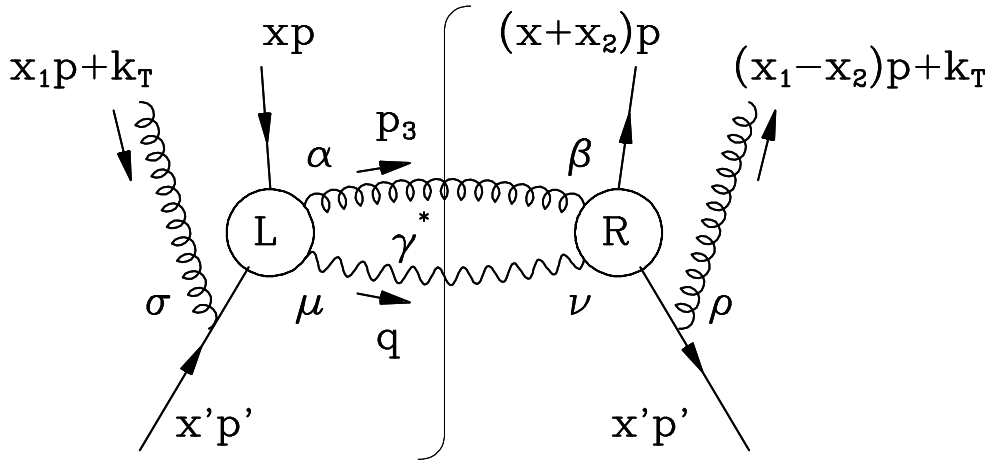


(a)

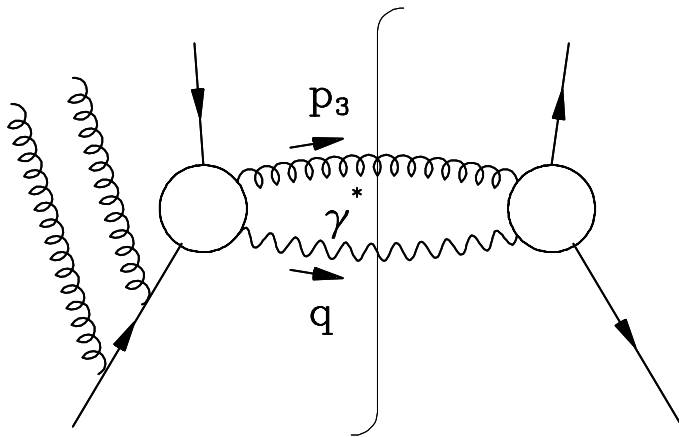


(b)

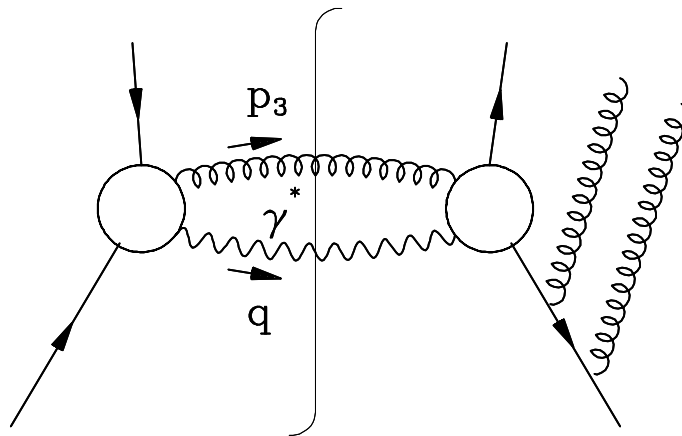
Fig. 3



(a)



(b)



(c)

Fig.4

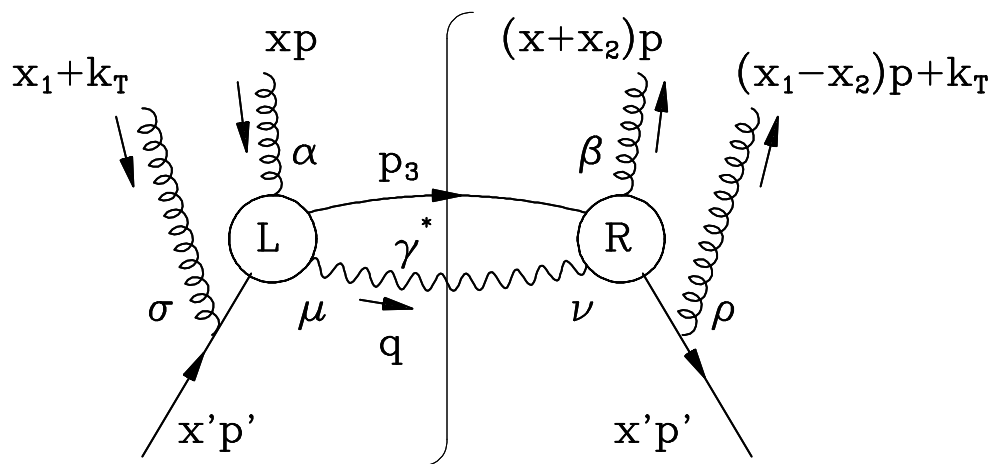


Fig. 5

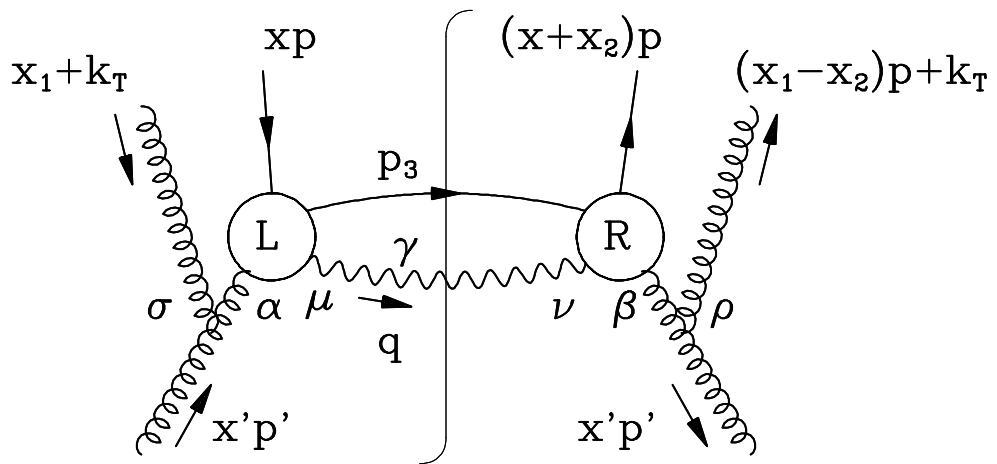


Fig. 6

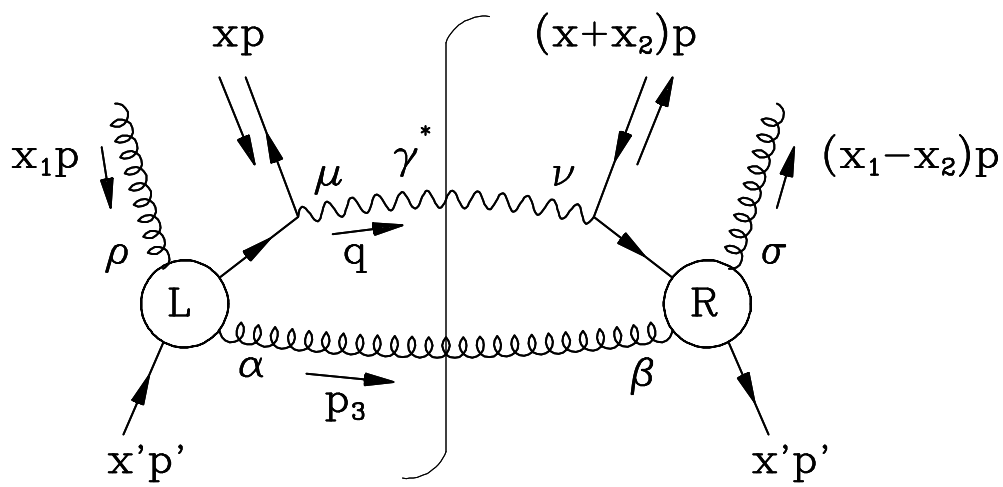


Fig. 7

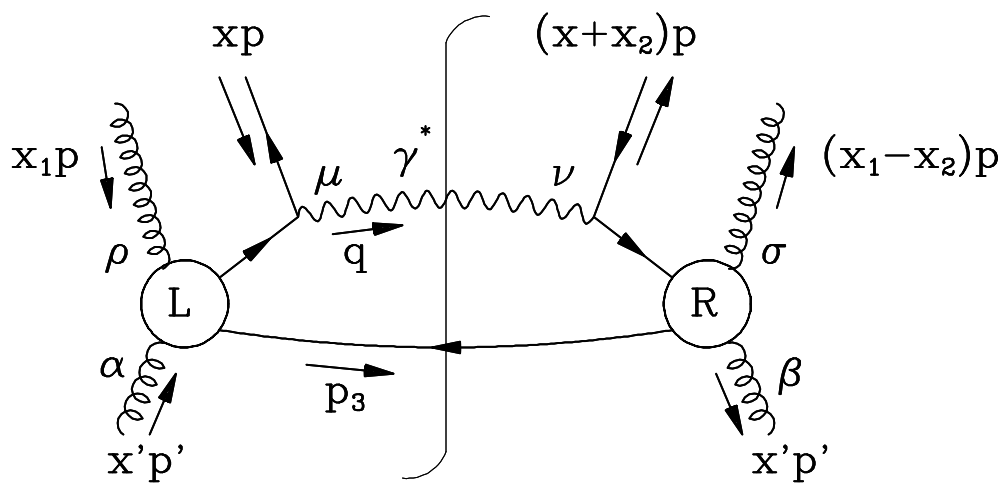


Fig. 8

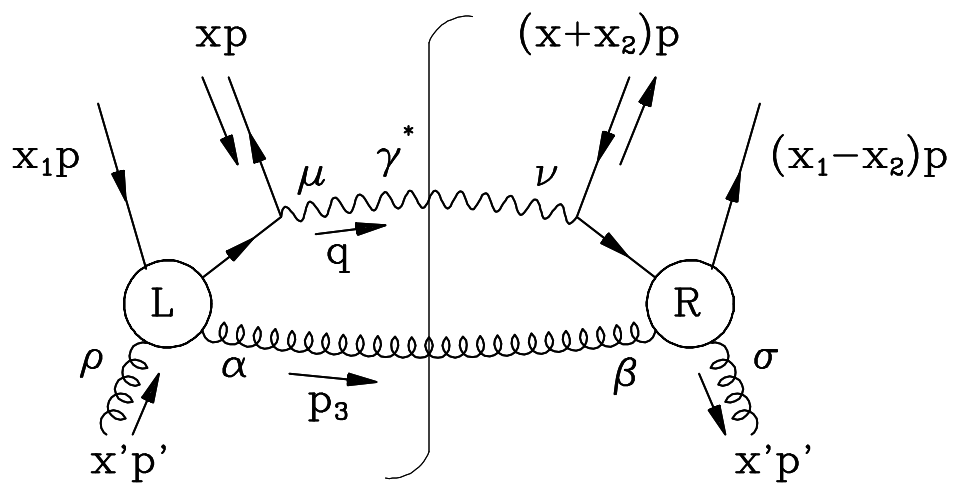
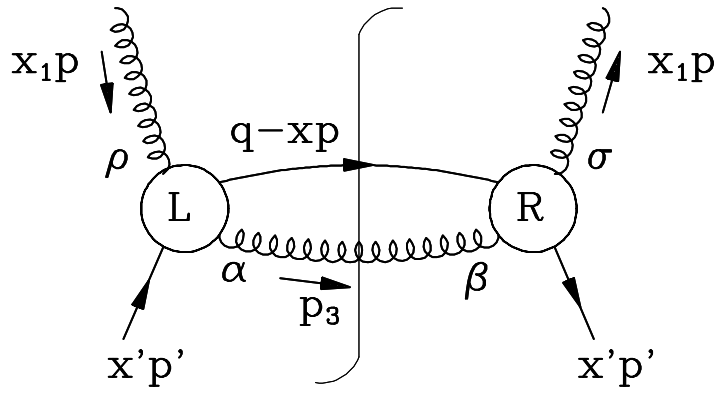
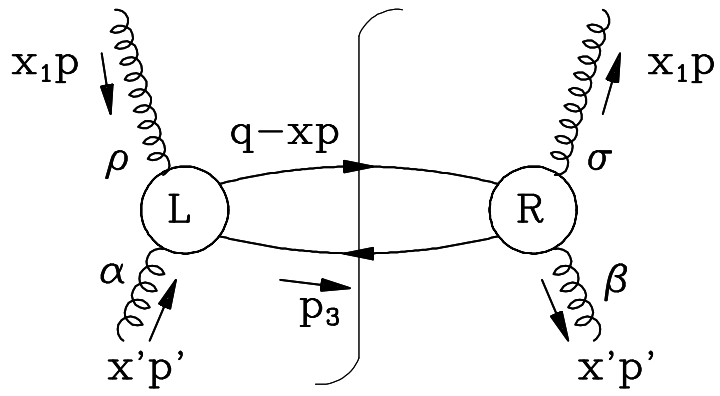


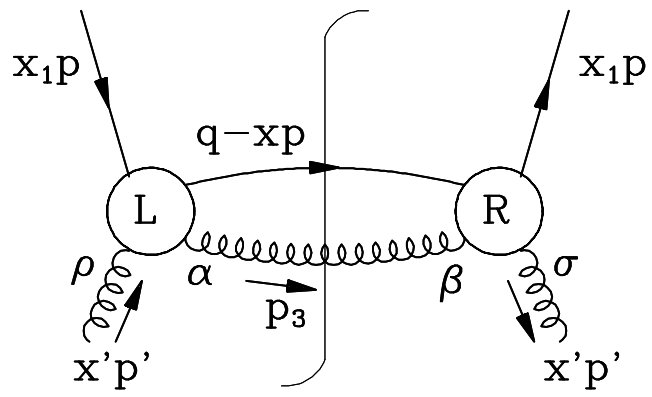
Fig. 9



(a)



(b)



(c)

Fig.10

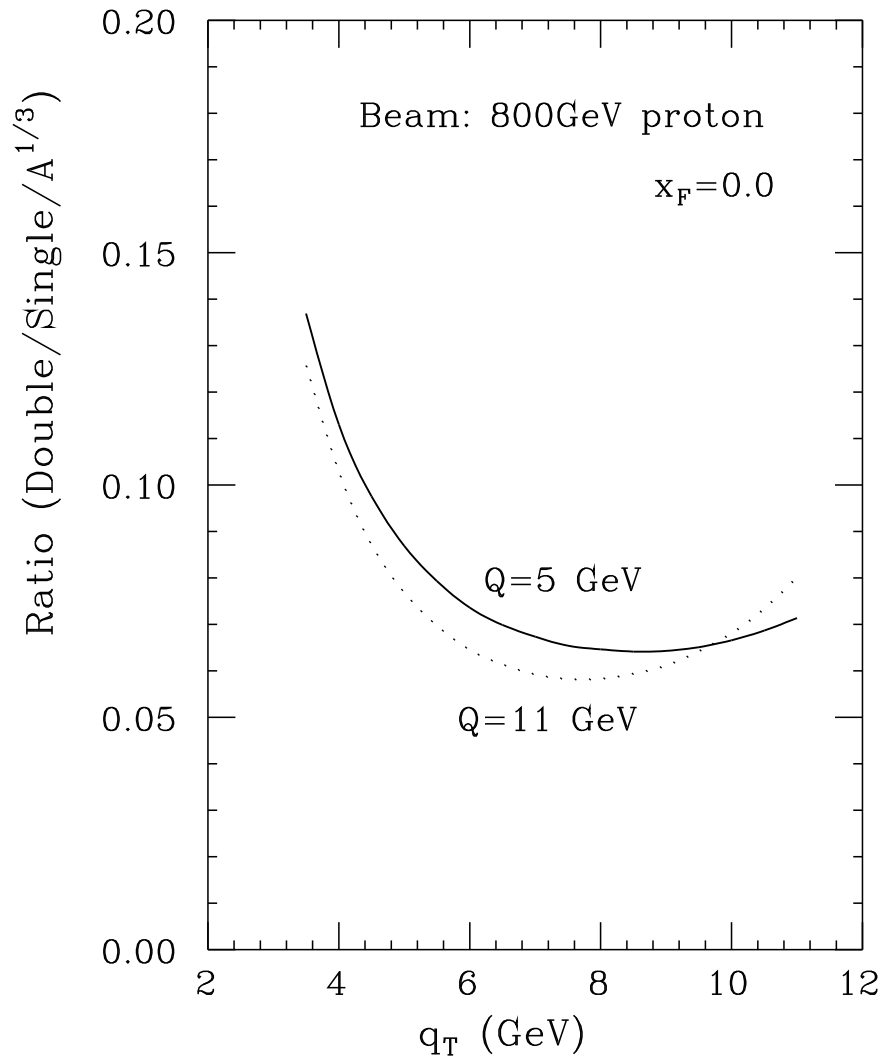


Fig. 11

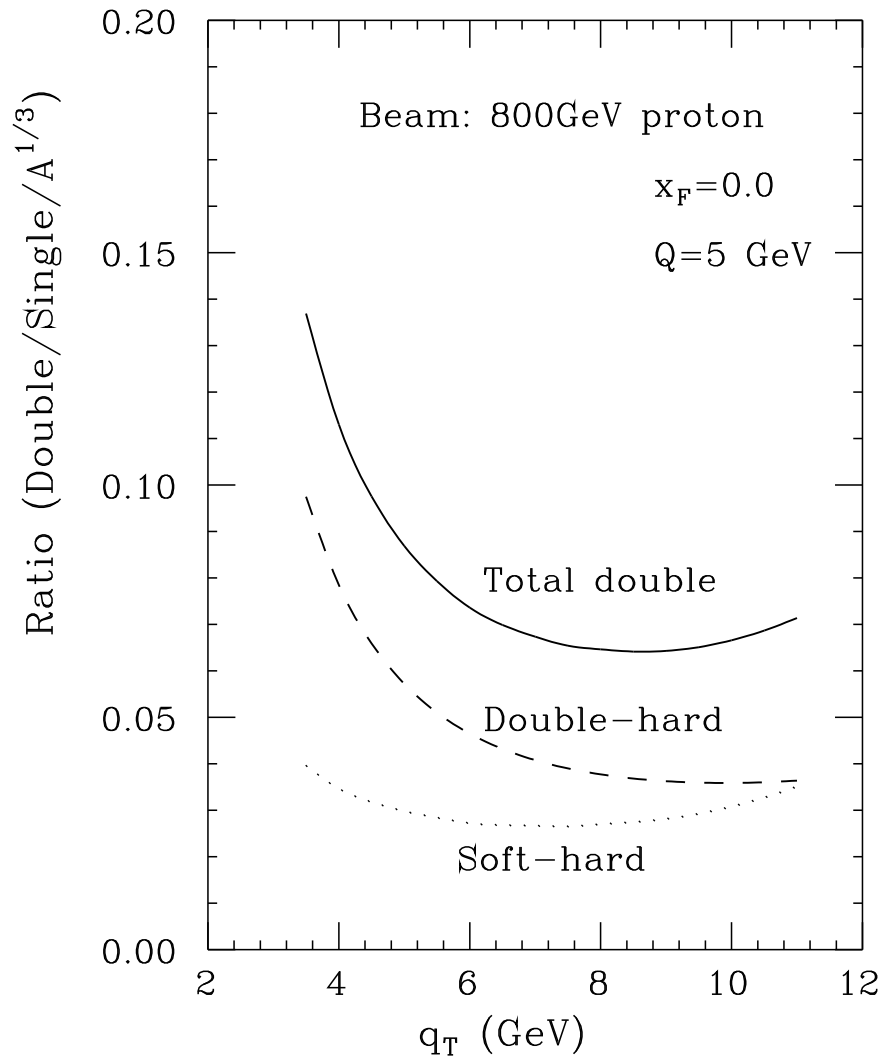


Fig. 12

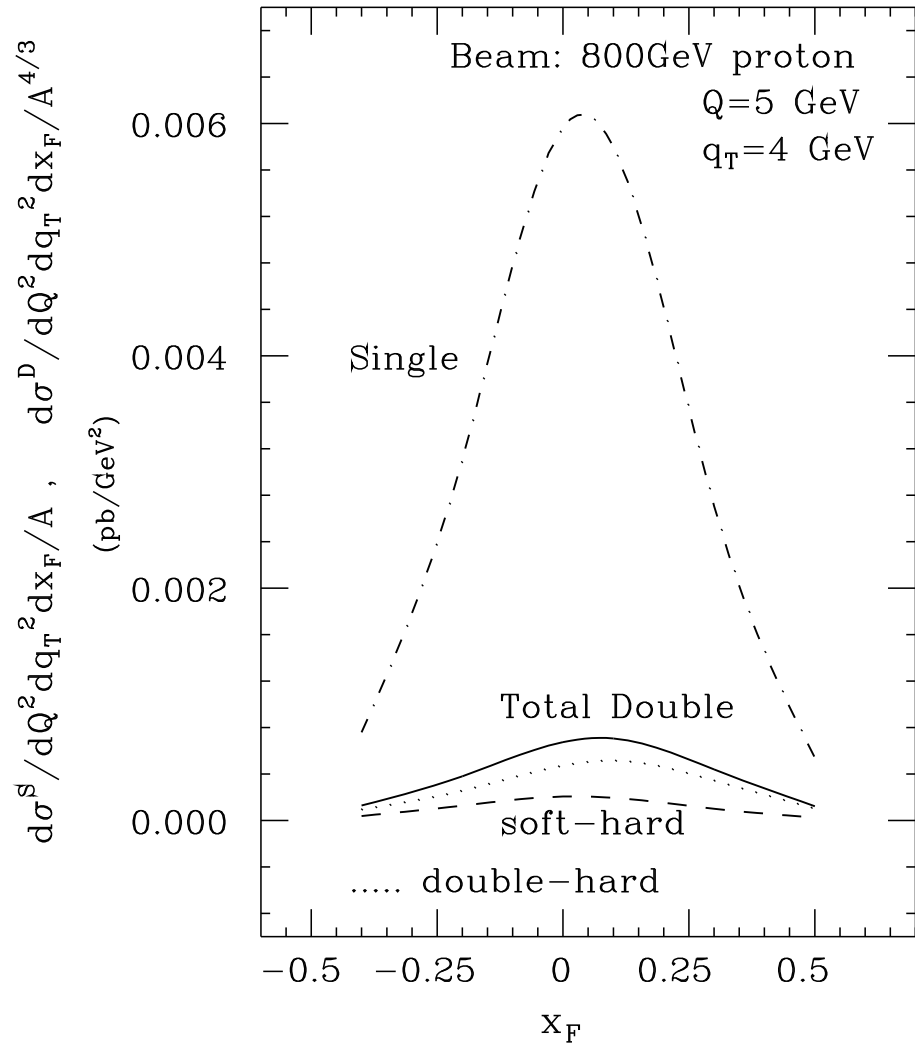


Fig. 13

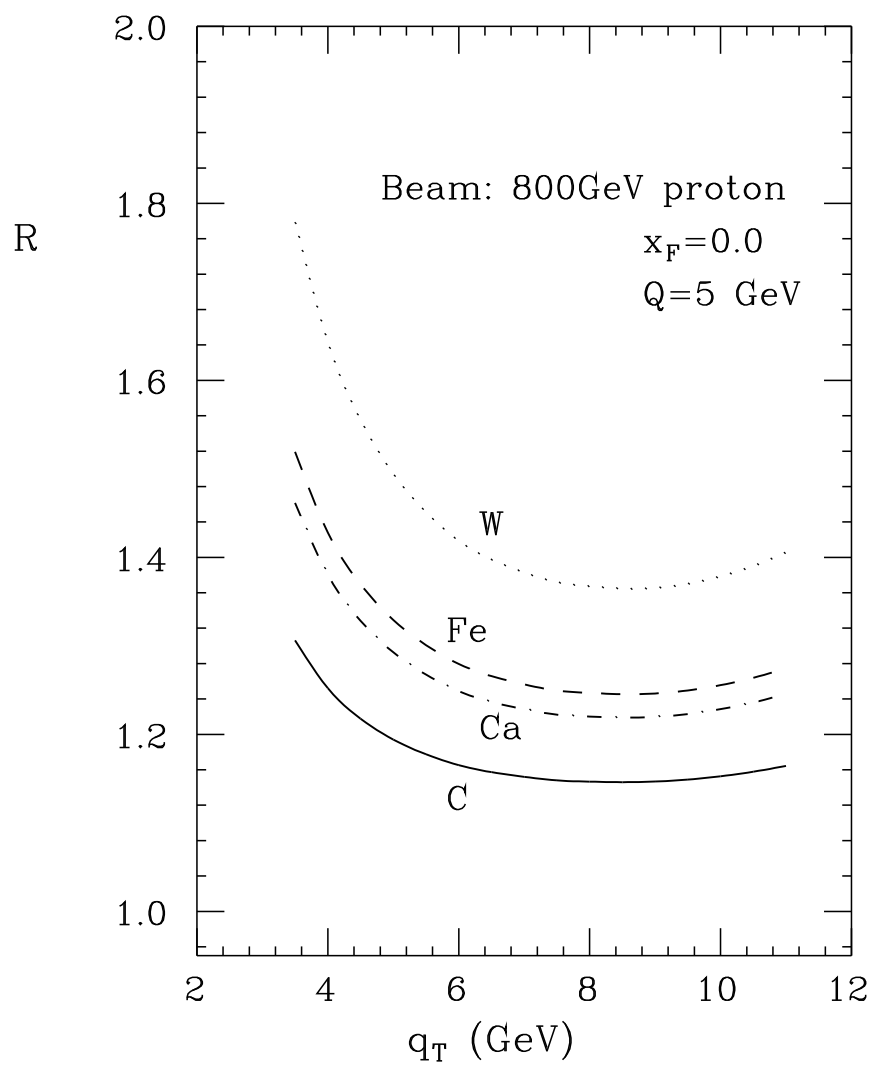


Fig. 14

Expected double scattering at small q_T

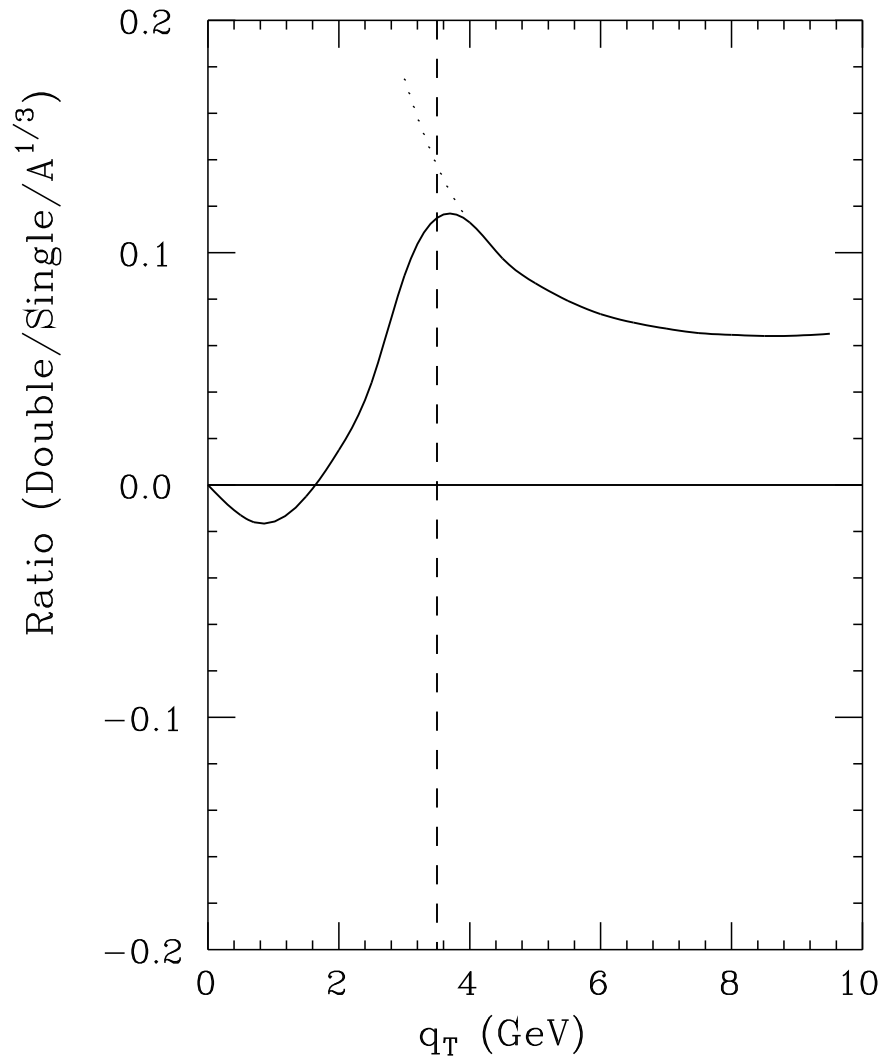


Fig. 15